[American Journal of Science, Vol. 308, March, 2008, P. 270–303, DOI 10.2475/03.2008.04]

SHRIMP U–Pb ZIRCON GEOCHRONOLOGY OF THE HUAI'AN COMPLEX: CONSTRAINTS ON LATE ARCHEAN TO PALEOPROTEROZOIC MAGMATIC AND METAMORPHIC EVENTS IN THE TRANS-NORTH CHINA OROGEN

GUOCHUN ZHAO*†, SIMON A. WILDE**, MIN SUN*, JINGHUI GUO***, ALFRED KRÖNER§, SANZHONG LI§§, XUPING LI§§§, and JIAN ZHANG*

ABSTRACT. The Huai'an Complex is situated in the northern segment of the Trans-North China Orogen (TNCO), a continent-continent collisional belt along which the discrete Archean Eastern and Western Blocks amalgamated to form the basement of the North China Craton. The complex consists of six distinct lithologic units: the Huai'an TTG gneisses, the Manjinggou high-pressure mafic granulites, the Khondalite Series, the Dongjiagou granitic gneiss, the Huai'an charnockite, and the Dapinggou K-feldspar granite. SHRIMP U–Pb geochronology, combined with Th and U data and cathodoluminescence (CL) imaging of zircons, enables resolution of magmatic and metamorphic events that can be directed towards understanding the late Archean to Paleoproterozoic history of the TNCO. CL images reveal the coexistence of magmatic and metamorphic zircons in most lithologies of the Huai'an Complex, of which the metamorphic zircons occur as either single grains or overgrowth rims surrounding and truncating oscillatory-zoned magmatic zircon cores. SHRIMP U–Pb analyses on magmatic zircons reveal that the tonalitic, trondhjemitic and granodioritic protoliths of the Huai'an TTG gneisses were emplaced at 2515 ± 20 Ma, 2499 ± 19 Ma and 2440 ± 26 Ma, respectively, much earlier than the emplacement of the Dongjiagou granitic gneiss dated at 2036 ± 16 Ma. However, their metamorphic zircons yield similar concordant $^{207}Pb/^{206}Pb$ ages of 1847 ± 17 Ma, 1842 ± 10 Ma and 1847 ± 11 Ma for the tonalitic, trondhjemitic and granodioritic gneisses, respectively, and 1839 ± 46 Ma for the Dongjia granitic gneiss. These ages demonstrate that the Huai'an Complex underwent a regional metamorphic event at ~1850 Ma, which is further supported by a mean $^{207}Pb/^{206}Pb$ age of 1848 ± 19 Ma for metamorphic zircons in the Manjinggou high-pressure mafic granulite and 1849 ± 10 Ma and 1850 ± 17 Ma for igneous zircons in the anatectic Huai'an charnockite and Dapinggou garnet-bearing S-type granite, respectively. The timing of late Archean to Paleoproterozoic magmatism and regional metamorphism in the Huai'an Complex is in general agreement with recent SHRIMP zircon data for other metamorphic complexes in the TNCO. These data prove that the high-grade gneiss complexes were not the basement to the low-grade granite-greenstone terranes in the TNCO. Furthermore, the lithologies of the orogen are considered to have developed as a long-lived magmatic arc that was subsequently tectonically disrupted and juxtaposed during the collision of the Eastern and Western Blocks at ~1.85 Ga, leading to final assembly of the North China Craton.

INTRODUCTION

A recent tectonic model for the Precambrian evolution of the North China Craton envisages discrete Archean Eastern and Western Blocks that developed independently and then amalgamated along the Trans-North China Orogen (TNCO) (fig. 1) (see Zhao and others, 2007 and references cited therein). However, there is still debate

*Department of Earth Sciences, University of Hong Kong, Pokfulam Road, Hong Kong
**Department of Applied Geology, Curtin University of Technology, GPO Box U1987, Perth, 6845, Australia
***Institute of Geology and Geophysics, Chinese Academy of Sciences, Beijing, 100029, China
§Institut für Geowissenschaften, Universität Mainz, 55099 Mainz, Germany
§§College of Marine Geosciences, Ocean University of China, 266003, Qingdao, China
§§§College of Geoinformation Science and Engineering, Shandong University of Science and Technology, Qingdao, 266510, China
†Corresponding author: E-mail: gzhao@hkucc.hku.hk

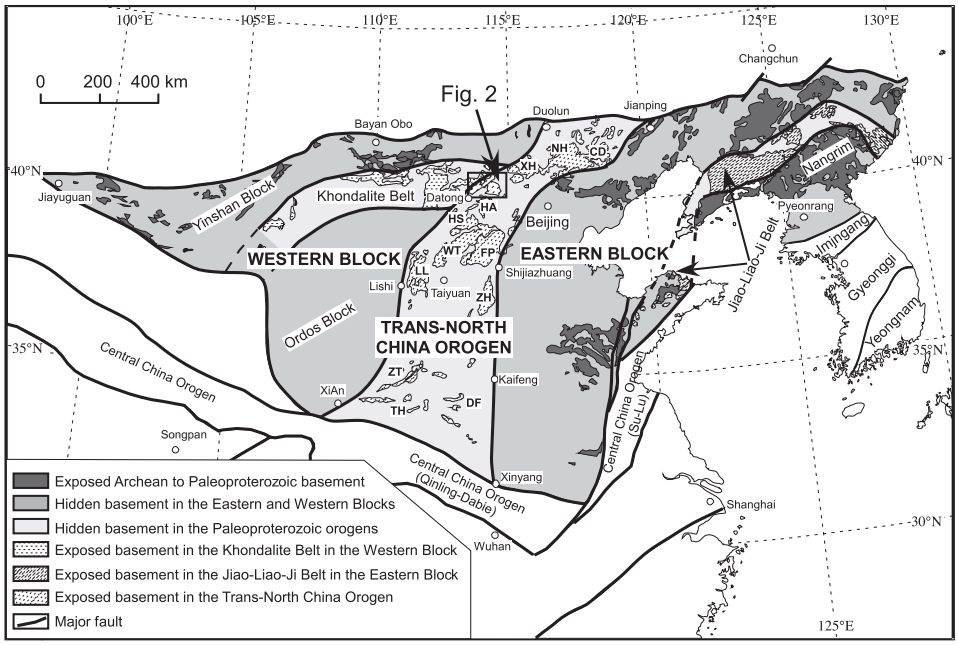

Fig. 1. Tectonic subdivision of the North China Craton, modified from Zhao and others (2005). Abbreviations for metamorphic complexes: CD – Chengde; DF – Dengfeng; HA – Huai'an; LL- Lüliang; TH – Taihua; WT – Wutai; XH – Xuanhua; ZH – Zanhuang; ZT – Zhongtiao. Figure 2 is outlined.

surrounding the timing of collision between the Eastern and Western Blocks, with one school of thought proposing that the collision occurred at ~2.5 Ga, whereas others believe that the final amalgamation of the two blocks was completed at ~1.85 Ga (see Zhao and others, 2007 for detailed discussion). This controversy results from the lack of reliable isotopic ages, especially of metamorphic events, which has hampered further understanding of the history of the North China Craton. To resolve this issue, extensive zircon dating of rocks in the Hengshan-Wutai-Fuping mountain belt has been carried out, a representative basement exposure across the middle segment of the TNCO (fig. 1, see Zhao and others, 2007 for summary and references). Some major conclusions from these data are summarized as follows: (1) high-pressure granulites and eclogites in the Hengshan Complex are strongly deformed gabbroic dikes that were emplaced at ~1.92 Ga and experienced high-pressure metamorphism at ~1.85 Ga (Kröner and others, 2005a, 2005b, 2006); (2) ductilely deformed Paleoproterozoic granitoid gneisses in the Hengshan and Fuping Complexes were emplaced between 2359 and 2024 Ma, indicating that the main deformation in these areas is not Archean but Paleoproterozoic in age (Guan and others, 2002; Zhao and others, 2002; Kröner and others, 2005a, 2005b); and (3) metamorphic zircons are present in both the Archean and Paleoproterozoic rocks of the Hengshan and Fuping Complexes and yield consistent metamorphic ages of ~1.85 Ga (Guan and others, 2002; Zhao and others, 2002; Kröner and others, 2005a, 2005b, 2006). These new geochronological data clearly support the model that collision between the Eastern and Western Blocks occurred at ~1.85 Ga and not at ~2.5 Ga. This conclusion is also supported by recent age data for the Taihua Complex in the southern segment of the TNCO (Wan and others, 2006). However, all these investigations are limited to the middle and southern segments of the TNCO, whereas it remains unknown whether the northern part of the orogen experienced the same tectono-thermal history. In this contribution, we carried

out SHIRMP U-Pb zircon dating on representative rocks of the Huai'an Complex, a key area in the northern part of the TNCO, where high-pressure mafic granulites/retrograded eclogites were first discovered in the North China Craton (Zhai and others, 1993). Our new ages enable an evaluation of the timing of collision and thereby place rigorous constraints on several key issues related to the late Archean to Paleoproterozoic accretion and assembly of the North China Craton.

REGIONAL SETTING

Lithological, geochemical, structural, metamorphic and geochronological differences between basement rocks of the Eastern and Western Blocks and the TNCO have been summarized by Zhao and others (2001a) and are not repeated here. This three-fold subdivision of the North China Craton has been further refined and modified using new structural, petrological and geochronological data (Zhao and others, 2003, 2005). These data suggest that the Western Block formed by amalgamation of the Ordos Terrane in the south and the Yinshan Terrane in the north along the east-west-trending Khondalite Belt (fig. 1) at 1.90 to ~1.95 Ga, about 50 to 100 Ma earlier than the collision of the Western and Eastern Blocks (Zhao and others, 2005). The data also suggest that the Eastern Block underwent Paleoproterozoic rifting along its eastern continental margin in the period 2.2 to 1.9 Ga, forming the Jiao-Liao-Ji Rift Belt (fig. 1; Li and others, 2004a, 2004b, 2005, 2006).

The TNCO, a nearly south-north-trending zone up to ~1200 km long and 100 to 300 km wide (fig. 1), is separated from the Eastern and Western Blocks by the Xingyang-Kaifeng-Shijiazhuang-Jiianping Fault and the Huashan-Lishi-Datong-Duolun Fault, respectively. Both faults strike N-S in the central and southern parts and NE-SW in the north. The main lithotectonic features of the TNCO include: (1) dominant late Archaean to Palaeoproterozoic arc-related juvenile crust with minor reworked basement rocks (Zhao and others, 1999a, 2000a; Liu and others, 2002, 2004, 2005; Wilde and others, 2002, 2004a, 2005; Wilde and Zhao, 2005; Wu and others, 2005); (2) linear structural belts defined by strike-slip ductile shear zones, large-scale thrusting and folding, and transcurrent tectonics (Li and Qian, 1991; Zhang and others, 1994; Dirks and others, 1997; Wang and others, 2003, 2004, 2007; Zhang and others, 2007); (3) sheath folds and mineral lineations (Wu and Zhong, 1998; Zhang and others, 2007); (4) high-pressure granulites and retrograde eclogites (Zhai and others, 1993, 1996; Zhao and others, 2001b; Guo and others, 2002, 2005; O'Brien and others, 2005; Zhang and others, 2006); (5) clockwise metamorphic P-T paths involving near-isothermal decompression (Guo and others, 1993, 1996, 2001; Zhai and others, 1993; Mei, 1994; Guo and Shi, 1996; Liu, 1996; Liu and others, 1996; Zhao and others, 1999b, 2000b; Guo and Zhai, 2001; O'Brien and others, 2005); (6) ancient oceanic fragments and ophiolitic mélange (Li and others, 1990; Bai and others, 1992; Wang and others, 1996, 1997); (7) syn- or post-tectonic granites (Tian, 1991); and (8) post-collisional mafic dike swarms (Hall and others, 2000). Most of these lithotectonic elements are classical indicators of collision tectonics.

The Huai'an Complex is situated in the central-north segment of the TNCO (fig. 1), north of the Hengshan Complex and southwest of the Xuanhua Complex (fig. 2), both of which contain high-pressure granulites or retrograded eclogites (Zhao and others, 2001b; Guo and others, 2002; O'Brien and others, 2005). West of the Huai'an Complex is the Jining Complex which forms the easternmost part of the Paleoproterozoic Khondalite Belt in the Western Block (fig. 2), and in which ultrahigh temperature metamorphic mineral assemblages were recently reported (Santosh and others, 2006, 2007). It consists of S-type granites and what is referred to as the "Khondalite Series", a supracrustal suite dominated by metapelites, calc-silicate rocks and marbles, and probably representing a stable continental margin deposit (Lu, 1991; Lu and Jin, 1993). Separating the Huai'an and Jining Complexes is a detachment fault that is

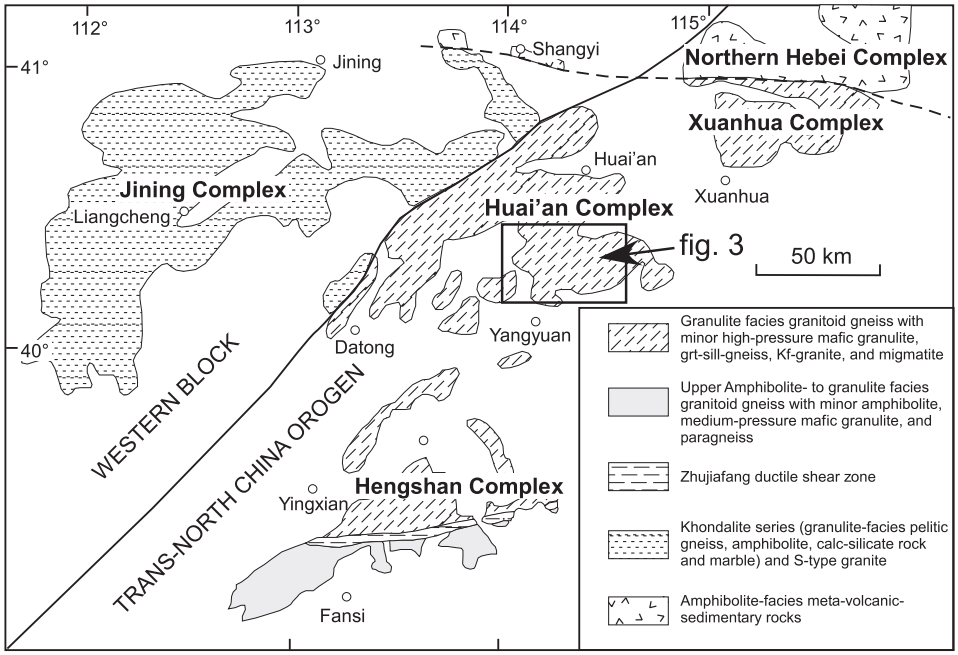

Fig. 2. Spatial relationships of the Huai'an Complex with adjacent Hengshan, Xuanhua and Jining complexes in the TNCO.

considered to have accommodated extension after crustal thickening (Zhang and others, 1994; Wu and Zhong, 1998; Guo and others, 2002).

LITHOLOGIES OF THE HUAI'AN COMPLEX

The Huai'an Complex comprises six distinct lithologic units: (1) the Huai'an TTG gneisses, (2) the Manjinggou high-pressure mafic granulites, (3) the Khondalite Series, (4) the Dongjiagou granitic gneiss, (5) the Huai'an enderbite and charnockite, and (6) the Dapinggou granite (Zhang and others, 1994; Liu, ms, 1995; Guo and others, 2002). Large-scale mapping of these lithologic units is on-going, but in the Manjinggou area, where HP mafic granulites were first discovered (Zhai and others, 1993), most of these lithologies have been mapped out as shown in figure 3 (Guo and others, 2002).

Of these lithologies, the Huai'an TTG gneisses make up ~60 percent of the complex and consist of dioritic, tonalitic, trondhjemitic and granodioritic gneisses that have undergone a complex history of upper amphibolite- to granulite-facies metamorphism and intense polyphase deformation (Zhang and others, 1994). The typical mineral assemblage of the TTG gneisses is plagioclase + quartz + biotite + hornblende + orthopyroxene + clinopyroxene ± garnet ± opaque minerals. These rocks have geochemical characteristics similar to high-grade gray gneisses elsewhere in the world (Guo and others, 1993, 1996; Guo and Shi, 1996). On the basis of petrological and geochemical data, Guo and others (1996) proposed that the Huai'an TTG gneisses were derived from partial melting of garnet-bearing mafic granulites or eclogites.

The Manjinggou HP mafic granulites occur in boudins and sheets, ranging from 0.1 to 2 m in width and 0.1 to 50 m in length, within the heterogeneous veined and deformed granulite-facies TTG gneisses, though some intensively retrograded HP granulitic xenoliths are also found in the Huai'an charnockites, Dongjiagou granitic

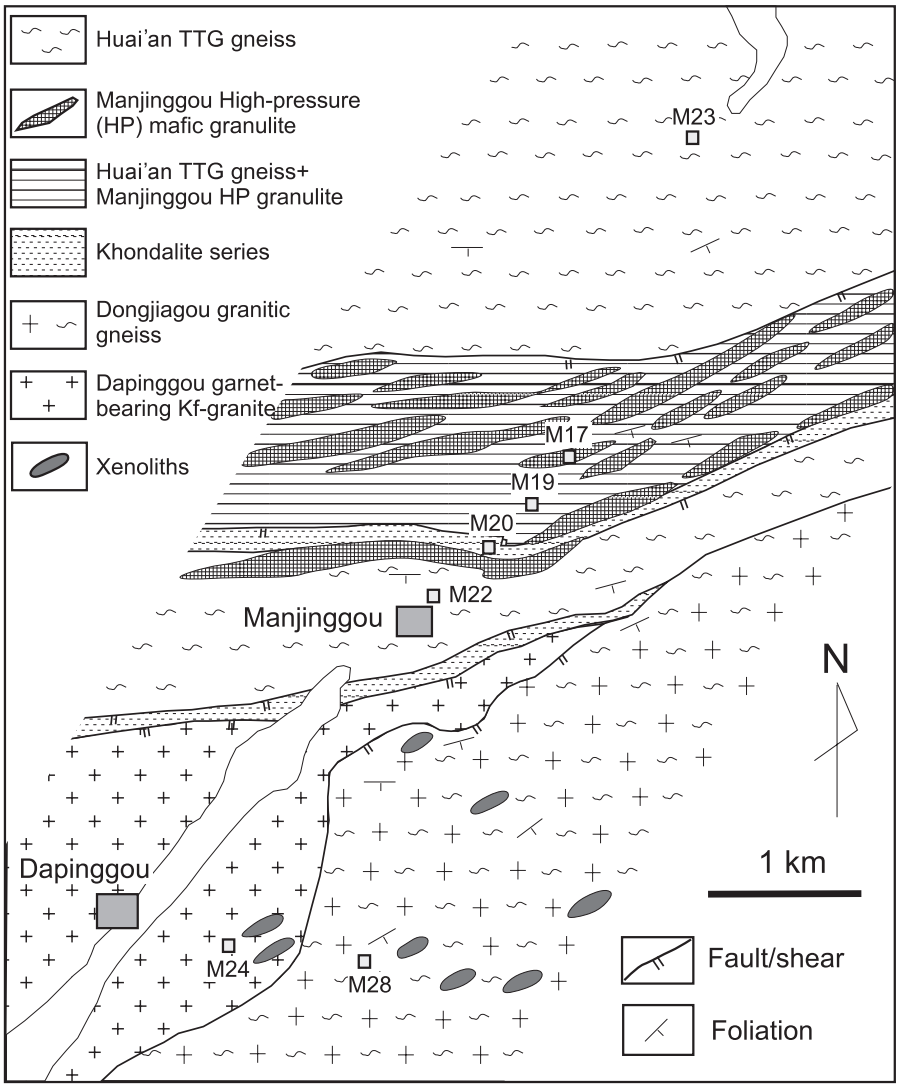

Fig. 3. Contribution of the Huai'an TTG gneisses, the Manjinggou high-pressure mafic granulite, the Khondalite Series, the Dongjiagou granitic gneiss, the Huai'an enderbite and charnockite, and the Dapinggou garnet-bearing S-type granite in the Manjinggou area (after Guo and others, 2002).

gneisses and Dapinggou K-feldspar granite (fig. 3; Guo and others, 2002). Generally, there is a sharp contact between the HP mafic granulites and the TTG gneisses, but no obvious intrusive relationships are observed between them in the field. The long axes of the HP granulite boudins are always parallel to the foliation of the TTG gneisses. In rare cases, and especially in low-strain zones, the HP granulite boudins and sheets can be intermittently traced for several hundred meters (fig. 3), which suggests that they were derived from metamorphosed gabbroic dikes. Ductile deformation has later rotated these dikes into parallelism with the layering in the enclosing gneisses and, at the same time, caused boudinage. This is the same as with the HP granulites in the Hengshan Complex (Kröner and others, 2005a, 2005b, 2006) south of the Huai'an Complex.

The Manjinggou HP mafic granulites contain mineral assemblages similar to those of HP granulites and retrograded eclogites in the Hengshan Complex, though omphacite pseudomorphs, indicated by clinopyroxene + sodic plagioclase (An_{10-20}) symplectic intergrowths (Zhao and others, 2001b), have not been found in the Manjinggou HP granulites. Guo and others (2002) recognized prograde (M_1), peak (M_2), post-peak decompression (M_3), and later cooling (M_4) metamorphic assemblages in the Manjinggou HP granulites. The prograde assemblage (M_1) is represented by low-Ca cores to growth-zoned garnet and associated inclusions of clinopyroxene, plagioclase and quartz, which formed under P-T conditions of ~10 kbar and 700°C. The peak assemblage (M_2) comprises high-Ca domains in garnet interiors and inclusions of clinopyroxene, plagioclase and quartz, yielding P-T conditions of 11 to 14.5 kbar and 750 to 870°C. The post-peak decompression assemblage (M_3) is represented by coronas and kelyphites (symplectites) of orthopyroxene + plagioclase + magnetite around garnet porphyroblasts, produced at conditions between 8.5 to 10.5 kbar and 770 to 830°C. The later cooling assemblage (M_4) includes hornblende + plagioclase kelyphites around garnet and formed at 5.5 to 8 kbar and 500 to 650°C. These mineral assemblages and their P-T estimates define a clockwise P-T path involving isothermal decompression (ITD) and cooling following peak metamorphism (fig. 4), which is considered to record the subduction and collision between the Eastern and Western Blocks (Guo and others, 2002; Zhang and others, 2006).

The Khondalite Series is mainly composed of graphite-bearing sillimanite-garnet gneiss, garnet quartzite, felsic paragneiss, calc-silicate rock and marble, which were derived from a sedimentary sequence metamorphosed at medium- to low-P granulite-facies conditions (Liu, ms, 1995). Interlayered with the Khondalite Series rocks are the

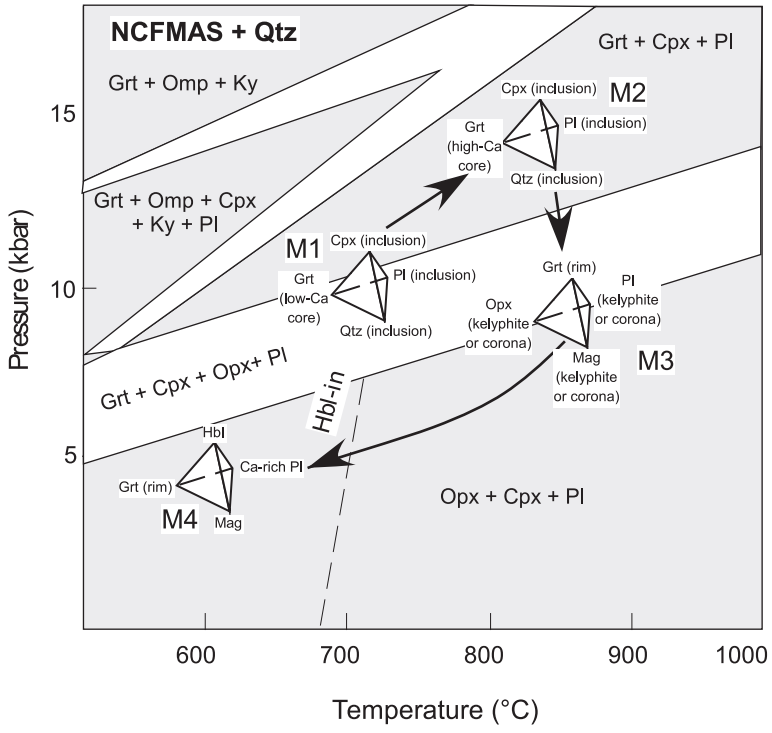

Fig. 4. P-T path for the Manjinggou high-pressure mafic granulites (revised after Guo and others, 2002).

Huai'an TTG gneisses, mafic granulites, syntectonic charnockites and S-type granites, and the boundaries between the Khondalite Series and other lithologic units are tectonic (Guo and others, 2002). Zhao and others (2005) suggested that the Khondalite Series rocks in the Huai'an Complex are allochthonous; they were part of the Jining Complex situated in the easternmost segment of the Paleoproterozoic Khondalite Belt in the Western Block and were thrust over the TNCO during collision of the Western and Eastern Blocks.

The Dongjiagou granitic gneiss only occurs in the southeastern part of the Manjinggou area and consists of pethitic K-feldspar (~45%), plagioclase (~20%), quartz (~20%), hornblende (~10%), garnet (~3%) and magnetite/ilmenite (~2%). Hornblende crystals show a strongly preferred orientation and define a gneissic fabric. It remains unknown whether hornblende is of metamorphic or igneous origin. The nature of the boundary between the Dongjiagou granitic gneiss, the Huai'an TTG gneisses and the Dapingggou granite is tectonic.

The Huai'an enderbite and charnockite occur as small-scale stocks or patches within the Huai'an TTG gneisses. The enderbite is mineralogically and chemically intermediate between the dioritic/tonalitic gneiss and the charnockite. It contains plagioclase (~45%), quartz (~20%), orthopyroxene + clinopyroxene (~20%), K-feldspar (~10%) and biotite (~5%), and exhibits weak banding and gneissosity, which is more prominent on weathered than on fresh surfaces. The charnockite contains more abundant K-feldspar (>30%) and less plagioclase (<25%) than the enderbite and is structurally more homogeneous and massive. In the field, the transformation of dioritic/tonalitic gneiss to enderbite is evident from the diffuse boundaries that cross the gneissic foliation and banding. However, the charnockite shows a clear intrusive relationship with the TTG gneisses. All these features suggest that the enderbite and charnockite were produced by *in-situ* anatexis of the dioritic/tonalitic gneisses (Liu, ms, 1995).

The Dapinggou garnet-bearing K-feldspar granite only occurs in the southwestern part of the Manjinggou area (fig. 3) and is characterized by garnet (up to 10%) and minor sillimanite (<1%), with perthitic K-feldspar (~45%), plagioclase (20%) and quartz (~25%). The granite is mineralogically homogeneous and structurally massive, though locally it exhibits a weak foliation. These mineralogical and structural features indicate that the Dapinggou granite is a syn- or post-tectonic S-type granite that was derived from partial melting of pelitic gneisses of the Khondalite Series (Guo and others, 1996).

PREVIOUS GEOCHRONOLOGY

The age of the rocks and timing of metamorphic events in the Huai'an Complex are poorly constrained. Most of the existing dates are based on K–Ar, Rb–Sr and Sm–Nd analyses of minerals and whole-rock samples and conventional U–Pb multi-grain zircon geochronology (Guo and others, 1993; Guo and Shi, 1996). Age estimates range between 2600 to 1800 Ma, with a few ages older than 2600 Ma or younger than 1800 Ma (Kröner and others, 1987; Liu, ms, 1989). Using conventional isotope dilution techniques on zircon fractions, Guo and Shi (1996) obtained a U–Pb zircon age of 2402 +9/-7 Ma for a tonalitic gneiss. This age is now considered to be geologically meaningless, since CL images show that most zircons from the Huai'an TTG gneisses have an igneous core and a metamorphic rim and dissolution analysis may therefore represent mixed ages. Using the same method, Guo and Shi (1996) obtained a U–Pb zircon age of 1892 + 23/-19 Ma for a sillimanite-garnet-gneiss of the Khondalite Series. Again, this age is now interpreted to reflect mixing of igneous and metamorphic zircons, since CL images show that most detrital zircons in the high-grade pelitic gneisses have metamorphic rims. In addition, an upper Concordia intercept zircon age of 2144 + 47/-36 Ma was obtained for the Dapinggou K-feldspar granite, and was interpreted to reflect emplacement of the granite (Guo and Shi,

1996). However, this age is likewise unreliable, because all data points are strongly discordant due to significant lead loss. The age of the Huai'an syn-tectonic charnockite has not been precisely determined, though three zircon grains yielded apparent $^{207}Pb/^{206}Pb$ ages of 1799 Ma, 1806 Ma and 1856 Ma, with a mean $^{207}Pb/^{206}Pb$ age of 1820 Ma (Guo and Shi, 1996).

Compared with other lithologies, the HP mafic granulites of the Huai'an Complex are well dated (Guo and others, 1993, 1996; Guo and Shi, 1996). Guo and others (1993) obtained a garnet-clinopyroxene-orthopyroxene Sm–Nd isochron age of 1824 ± 18 Ma and a U–Pb zircon age of 1833 ± 23 Ma, both interpreted to reflect a high-pressure metamorphic event. More recently, Guo and others (2005) SHRIMP-dated zircons from two HP mafic granulite samples collected from Manjinggou, and the metamorphic zircons yielded mean $^{207}Pb/^{206}Pb$ ages of 1817 ± 12 Ma (n = 20; MSWD = 0.65) and 1817 ± 12 Ma (n = 21; MSWD = 1.9), both interpreted as the age of the high-pressure metamorphic event. Whereas these SHRIMP results provide reliable data for peak metamorphism in the Manjinggou HP mafic granulites, significant questions still remain because of a lack of precise and reliable isotopic age data for other major lithologies of the Huai'an Complex.

SAMPLE SELECTION AND ANALYTICAL METHODS

Seven samples representing all major lithologies of the Huai'an Complex were selected for study. Of these, samples M21, M19 and M23 are two-pyroxene-bearing tonalitic, trondhjemitic and granodioritic gneisses, respectively, collected from the Huai'an TTG gneisses; sample M17 is a high-pressure mafic granulite collected from the Manjinggou area; sample M28 is from the Dongjiagou granitic gneiss; sample M22 is a massive charnockite; and sample M24 is from the Dapinggou garnet-bearing granite. Table 1 lists major petrographic features of each sample, and sample sites are shown on figure 3.

The samples were processed for heavy mineral separation by crushing and initial heavy liquid and subsequent magnetic separation. Samples were divided into size and magnetic fractions using a Frantz isodynamic separator. Zircons from the 105 to 132 and >132 μm non-magnetic fractions were hand-picked and mounted on adhesive tape, enclosed in epoxy resin and then polished to about half their thickness and photographed in reflected and transmitted light. Cathodoluminescence (CL) imaging of zircon grains was then carried out using a scanning electron microprobe at the Guanzhou Institute of Geochemistry. The mount was then cleaned and gold-coated. U–Th–Pb analyses were made on the exposed zircon surfaces using the Western Australian Consortium SHRIMP II ion microprobe housed at Curtin University, whose instrumental performance has been documented by De Laeter and Kennedy (1998). Detailed analytical procedures are described by Nelson (1997). Isotopic ratios are monitored by reference to a $^{206}Pb/^{238}U$ ratio of 0.09143 that is equivalent to an age of 564 Ma for the Sri Lankan gem zircon standard CZ3 (Pidgeon and others, 1994), fragments of which were mounted on each sample. Pb/U ratios in the unknown samples were corrected using the ln(Pb/U)/ln(UO/U) relationship as measured in standard CZ3. (This is all in Williams and Nelson.) Ages have been calculated from the U and Th decay constants recommended by Steiger and Jäger (1977). All reported ages represent $^{207}Pb/^{206}Pb$ data corrected using measured ^{204}Pb. The analytical data were reduced and plotted using the Squid (1.0) and IsoplotEx 2.46 programs (Ludwig, 2001). Individual analyses in the data table and concordia plots are presented with 1σ error and uncertainties in pooled ages are quoted at the 2σ (95 % confidence) level, unless otherwise indicated.

RESULTS

Huai'an TTG gneiss (samples M21, M19 and M23).—Most zircons in Huai'an TTG gneiss samples M21, M19 and M23 are euhedral and prismatic in morphology as is

Table 1

Brief descriptions of the analyzed samples

Sample	Rock Name	Main Minerals	Fabric	Environment
M21	Tonalitic gneiss	Pl (55%) + Qtz (25%) + Opx + Cpx (15%) + Hbl/Bt (5%)	Medium-grained ; strong gneissosity	Pre-tectonic
M19	Trondhjemitic gneisses	Pl (60%) + Qtz (30%) + Opx + Cpx (5%) + Bt (5%)	Medium-grained; strong gneissosity	Pre-tectonic
M23	Granodioritic gneiss	Pl (45%) + Qtz (25%) + Kf (10%) + Opx + Cpx (5%) + Hbl/Bt (5%)	Medium-grained; strong gneissosity	Pre-tectonic
M17	High-pressure mafic granulite	Pl (40%) + Cpx (25%) + Grt (20%) + Qtz (5%) + Opx (symplectite, 5%) + Hbl (5%)	Granoblastic texture; massive or weak foliation	Pre-tectonic
M28	Hbl granitic gneiss	Kf (40%) + Qtz (25%) + Pl (25%) + Hbl (10%) + Grt (<1%)	Granoblastic texture; gneissosity	Pre-tectonic
M22	Charnockite	Kf (30%) + Qtz (25%) + Pl (25%) + Opx (10%) + Bt (10%)	Granular texture; massive structure	Syn-tectonic
M24	Grt granite	Kf (40%) + Qtz (25%) + Pl (25%) + Grt (10%)	Granular texture; massive structure	Syn-tectonic

commonly observed in zircons from magmatic rocks, but have been recrystallized or overgrown by thin rims. CL images show that zircons in these samples can be grouped morphologically into three types: (1) those with concentric, oscillatory zoning (fig. 5A); (2) those with concentric oscillatory-zoned cores with narrow (<10 μm) or wide (>20 μm), highly luminescent, structureless rims (figs. 5B and 5C); and (3) those with dark cores with wide, highly luminescent, structureless rims (fig. 5D). Based on morphology and the assumption that the zircon rims are generally younger than the cores that they overgrow, the structureless rims in type (2) and (3) zircons are considered to have formed through metamorphic recrystallization/overgrowth; type (1) zircons and the oscillatory-zoned cores in type (2) represent igneous grains; the dark cores in type (3) zircons represent unconsumed igneous zircon.

The SHRIMP analytical data for sample M21 are presented in table 2. Analytical points were positioned on three individual grains with concentric, oscillatory zoning; four concentric, oscillatory-zoned, igneous cores and seven highly luminescent, structureless, metamorphic zircon rims. In terms of Th-U chemistry, concentric, oscillatory zoning in igneous zircon is characterized by high Th/U ratios, whereas the high luminescent, structureless, metamorphic zircon rims have much lower Th contents (fig. 6A). On a concordia plot (fig. 7), seven analyses of igneous zircon (individual grains and zoned cores) are concordant or nearly concordant, and define a single population with a weighted mean $^{207}Pb/^{206}Pb$ age of 2515 ± 20 Ma (MSWD=5.5),

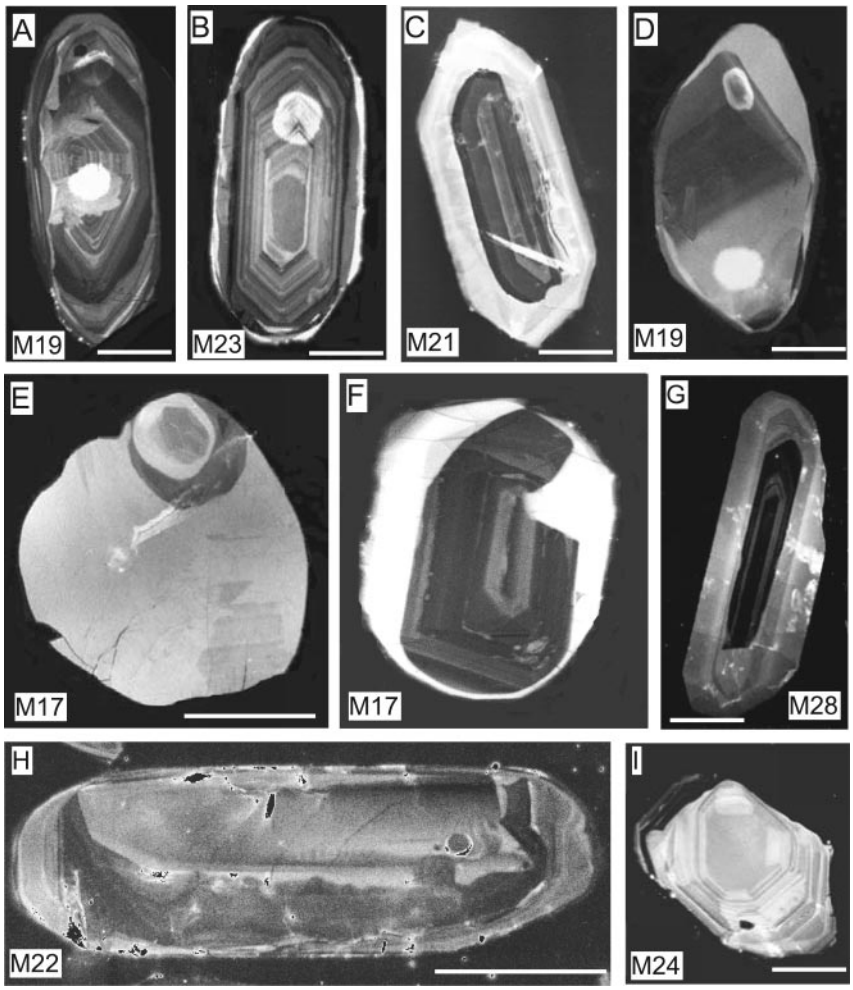

Fig. 5. Representative selection of CL zircon images of the studied samples. Descriptions of zircons are included in the text. All scale bars are 50 μm.

interpreted as the crystallization age of the igneous protolith of the tonalitic gneiss. Seven data points on the highly luminescent, structureless, metamorphic zircon rims are concordant to slightly discordant (fig. 7) and yielded a weighted mean $^{207}Pb/^{206}Pb$ age of 1847 ± 17 Ma (MSWD=3.8), interpreted as the time of metamorphic zircon growth.

For the trondhjemitic gneiss sample M19, analytical sites were positioned on 11 igneous and 10 metamorphic zircons. Most, but not all, metamorphic zircons are characterized by relatively low Th and high U contents, with most Th/U ratios lower than 0.2 (table 3), whereas all magmatic zircons show relatively high Th and low U contents, with most Th/U ratios higher than 0.6 (table 3; fig. 6B). On a concordia plot (fig. 8), 8 out of 11 analyses of the igneous zircons are concordant, or nearly concordant, and define a weighted mean $^{207}Pb/^{206}Pb$ age of 2499 ± 19 Ma (fig. 8), interpreted as the crystallization age of the igneous protolith of the trondhjemitic gneiss. The remaining three data points on igneous zircons are younger (fig. 8). These analyses may have overlapped the narrow metamorphic rims or have undergone

TABLE 2

U-Th-Pb SHRIMP data for sample M21 (tonalitic gneiss)

Spot	Texture	ppm U	ppm Th	$^{232}Th/^{238}U$	ppm $^{206}Pb^*$	$^{204}Pb/^{206}Pb$	% $^{206}Pb_c$	$^{207}Pb^*/^{206}Pb^*$	±%	$^{207}Pb^*/^{235}U$	±%	$^{206}Pb^*/^{238}U$	±%	err corr	% conc.	$^{207}Pb^*/^{206*}Pb$ age	
M021-1	(s)	75	58	0.79	31.0	3.9E-5	0.05	0.1684	0.79	11.13	2.5	0.480	2.4	.949	99	2541	±13
M021-4	(s)	70	54	0.81	28.7	1.0E-4	0.15	0.1618	0.80	10.69	2.5	0.479	2.4	.947	102	2475	±14
M021-10	(s)	201	217	1.12	81.3	4.1E-6	0.01	0.1645	0.55	10.69	2.4	0.471	2.3	.972	99	2502	± 9.3
M021-14	(r)	170	1	0.01	44.4	5.3E-5	0.08	0.1128	0.78	4.71	2.4	0.303	2.3	.948	92	1845	±14
M021-15	(r)	348	2	0.01	97.1	1.5E-5	--	0.1145	0.57	5.13	2.3	0.325	2.3	.970	97	1872	±10
M021-16	(r)	553	12	0.02	152	2.5E-6	--	0.1135	0.36	5.00	2.3	0.320	2.3	.987	96	1855	± 6.6
M021-17	(c)	287	203	0.73	119	3.0E-5	0.04	0.1699	0.66	11.34	2.4	0.484	2.3	.960	100	2556	±11
M021-18	(c)	310	217	0.72	122	3.9E-6	0.01	0.1653	0.38	10.46	2.3	0.459	2.3	.987	97	2511	± 6.3
M021-20	(c)	179	151	0.87	73.5	3.7E-5	0.05	0.1668	0.47	10.99	2.3	0.478	2.3	.980	100	2525	± 7.9
M021-21	(r)	492	52	0.11	137	4.1E-5	0.06	0.1114	0.43	4.99	2.3	0.325	2.3	.982	100	1822	± 7.9
M021-22	(r)	204	2	0.01	57.4	4.8E-5	0.07	0.1133	0.76	5.10	2.4	0.326	2.3	.949	98	1853	±14
M021-24	(r)	184	110	0.62	51.9	6.7E-5	0.10	0.1109	0.85	5.00	2.5	0.327	2.3	.938	101	1814	±15
M021-25	(r)	565	15	0.03	160	1.2E-5	0.02	0.1130	0.36	5.15	2.3	0.330	2.3	.987	100	1849	± 6.6
M021-27	(c)	691	671	1.00	271	1.7E-5	0.02	0.1644	0.51	10.35	2.3	0.457	2.3	.975	97	2501	± 8.7

Texture: (s) = single grains with concentric, oscillatory zoning (igneous zircon); (c) = concentric oscillatory-zoned core (igneous zircon); (r) = high luminescent, structureless rim (metamorphic zircon). Errors are 1-sigma; Pb_c and Pb indicate the common and radiogenic portions, respectively. Common Pb corrected using measured ^{204}Pb.

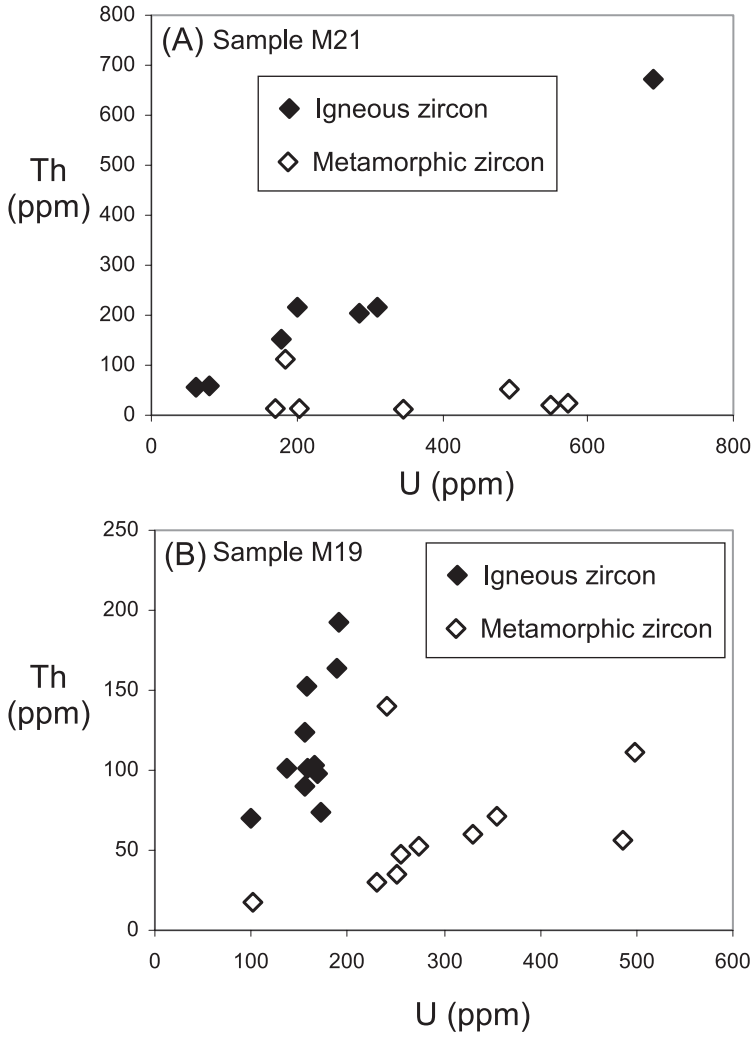

Fig. 6. Plots of Th vs U for the magmatic and metamorphic zircons in samples M21 and M19.

recrystallization during the later metamorphic event, yet still retain vestiges of original oscillatory zoning. Ten analyses of metamorphic zircon are mostly concordant but form two groups (fig. 8). One group consists of six analyses that define a weighted mean $^{207}Pb/^{206}Pb$ age of 1838 ± 35 Ma. The two concordant data points (spots 13 and 15; table 3) in this group give a mean age of 1842 ± 9 Ma (MSWD =2) (fig. 8), similar to the weighted mean $^{207}Pb/^{206}Pb$ age of metamorphic zircons in tonalitic gneiss sample M21, and are thus interpreted as reflecting the time of peak metamorphism. Another group consists of four analyses that have $^{207}Pb/^{206}Pb$ ages somewhat older than the other six data points, and define a weighted mean $^{207}Pb/^{206}Pb$ age of 1954 ± 32 Ma (fig. 8). There are two possible interpretations for this age. One is that these zircons record an earlier metamorphic event resulting from collision between the Ordos and Yinshan Terrane to form the Western Block, which is considered to have occurred before the collision of the Eastern and Western Blocks (Zhao and others, 2005). Another interpretation is that these analyses may be positioned on very narrow

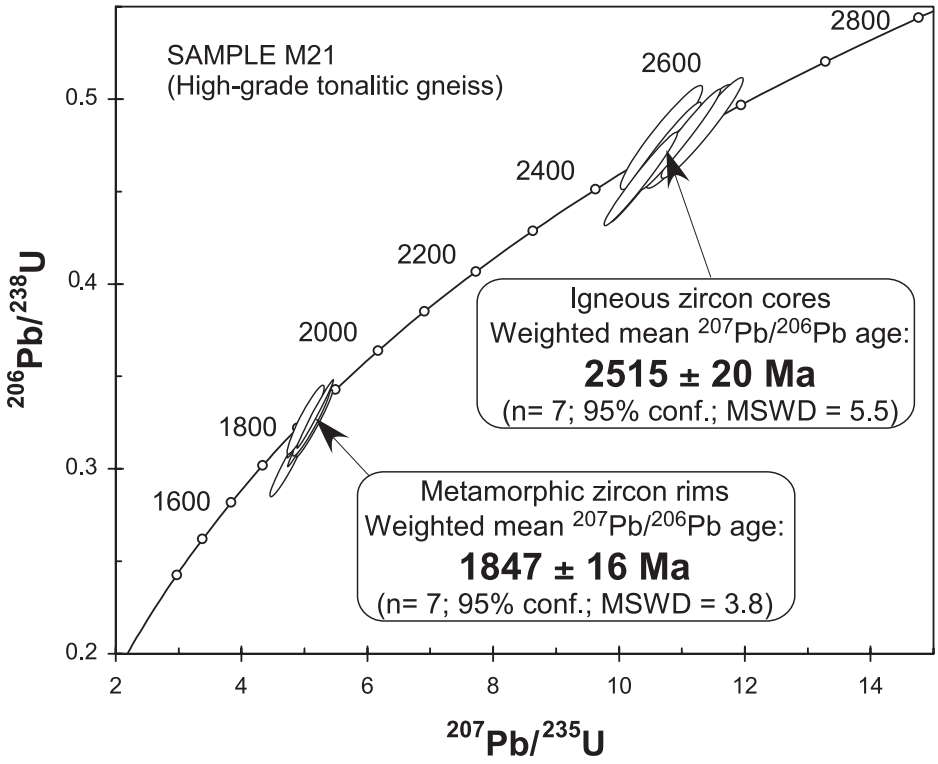

Fig. 7. Concordia plot of SHRIMP U-Pb zircon analytical results for the Huai'an tonalitic gneiss (sample M21). Errors are 1-sigma.

metamorphic zircon rims or overlap with the zoned zircon cores of magmatic origin, and thus these data points record mixed ages and are geologically meaningless.

SHRIMP analyses on two-pyroxene granodioritic gneiss samples M23 were made on seven oscillatorily-zoned igneous cores (Types 1 and 2), one dark core (Type 3) without obvious zoning, and eight structureless metamorphic rims that have overgrown Type 2 and 3 zircons (table 4). Unlike those in samples M23 and M19, most metamorphic zircon rims in sample M23 do not show low Th/U ratios (table 4), although two metamorphic zircon rims (for example spots 15, and 16) have extremely low Th/U ratios (<0.01). On a concordia plot (fig. 9), seven analyses on oscillatorily-zoned igneous cores form a reasonably concordant group with a weighted mean $^{207}Pb/^{206}Pb$ age of 2440 ± 26 Ma (MSWD = 2.7) (fig. 9), interpreted as the crystallization age of the gneiss protolith. One analysis (spot 14) on a dark zircon core gives an apparent $^{207}Pb/^{206}Pb$ age of 2581 ± 10 Ma (fig. 9), much older than other zircon cores and interpreted as recording the age of an inherited grain. Seven analyses on structureless rims form a well-defined concordant population with a weighted mean $^{207}Pb/^{206}Pb$ age of 1847 ± 11 Ma (MSWD = 0.97), similar to metamorphic ages obtained from the other two Huai'an TTG gneiss samples and thus interpreted reflect the time of metamorphic zircon growth in the Huai'an Complex.

Manjinggou HP granulite (sample M17).—Only a few zircon grains were present in sample M17 and CL images reveal two morphologically distinct types: one is nearly spherical, multifaceted, and structureless with high luminescence (fig. 6E), typical of a metamorphic origin; the other has dark (low-luminescence) oscillatorily-zoned cores

TABLE 3

U-Th-Pb SHRIMP data for sample M19 (trondhjemitic gneiss)

Spot	Texture	ppm U	ppm Th	$^{232}Th/^{238}U$	ppm $^{206}Pb^*$	$^{204}Pb/^{206}Pb$	% $^{206}Pb_c$	$^{207}Pb^*/^{206}Pb^*$	±%	$^{207}Pb^*/^{235}U$	±%	$^{206}Pb^*/^{238}U$	±%	err corr	% conc	$^{207}Pb^*/^{206}Pb^*$ age	
M19-1	M-I	499	111	0.23	141	2.8E-6	0.00	0.1187	0.45	5.38	7.6	0.328	7.6	.998	94	1937	± 8.0
M19-2	I	155	91	0.60	59.5	4.5E-6	--	0.1626	0.35	10.02	7.6	0.447	7.6	.999	96	2483	± 5.9
M19-3	I	166	97	0.60	62.5	4.4E-6	--	0.1616	0.61	9.76	7.7	0.438	7.7	.997	95	2472	±10
M19-4	I	158	153	1.00	62.2	5.2E-5	0.07	0.1665	0.68	10.50	7.6	0.458	7.6	.996	96	2522	±11
M19-5	M	486	57	0.12	134	1.7E-5	0.03	0.1145	0.33	5.08	7.6	0.322	7.6	.999	96	1873	± 6.0
M19-6	I	188	164	0.90	72.6	1.6E-5	0.02	0.1639	0.48	10.16	7.6	0.450	7.6	.998	96	2496	± 8.0
M19-7	I	164	100	0.63	58.7	1.1E-4	0.16	0.1562	0.77	8.98	7.6	0.417	7.6	.995	93	2415	±13
M19-8	I	160	101	0.65	60.0	5.5E-5	0.08	0.1581	0.70	9.52	7.6	0.436	7.6	.996	94	2436	±12
M19-10	M	231	30	0.14	68.8	4.4E-5	0.07	0.1211	0.79	5.79	7.6	0.346	7.6	.995	97	1973	±14
M19-11	M	354	71	0.21	109	4.0E-6	0.01	0.1230	0.75	6.08	7.6	0.358	7.6	.995	99	2000	±13
M19-12	M	251	35	0.14	69.2	4.2E-5	0.07	0.1129	0.50	4.99	7.6	0.321	7.6	.998	97	1846	± 9.1
M19-13	I	191	193	1.04	76.7	1.5E-4	0.22	0.1677	0.48	10.80	7.6	0.467	7.6	.998	97	2535	± 8.0
M19-14	M	102	18	0.18	28.5	1.4E-5	--	0.1120	0.73	5.04	7.7	0.326	7.6	.995	99	1833	±13
M19-15	I	155	123	0.82	62.7	4.1E-5	0.06	0.1624	0.44	10.53	7.6	0.470	7.6	.998	100	2481	± 7.4
M19-16	M	274	52	0.20	78.2	2.1E-5	0.03	0.1128	0.43	5.17	7.6	0.332	7.6	.998	100	1845	± 7.7
M19-17	I	100	70	0.72	41.1	2.6E-5	0.04	0.1669	0.54	10.97	7.6	0.477	7.6	.997	99	2527	± 9.1
M19-18	M	330	61	0.19	96.1	1.3E-5	0.02	0.1211	0.58	5.66	7.6	0.339	7.6	.997	95	1972	±10
M19-19	I	137	101	0.76	54.9	1.9E-5	--	0.1644	0.52	10.59	7.6	0.467	7.6	.998	99	2501	± 8.8
M19-20	M	240	140	0.60	69.2	3.4E-5	0.05	0.1097	0.50	5.08	7.6	0.336	7.6	.998	104	1795	± 9.1
M19-21	I	173	73	0.44	68.5	2.4E-5	0.03	0.1578	0.49	10.04	7.6	0.461	7.6	.998	101	2433	± 8.2
M19-22	M	255	48	0.19	71.5	9.9E-6	0.02	0.1099	0.46	4.95	7.6	0.327	7.6	.998	101	1797	± 8.3

M = metamorphic zircon: high luminescence, structureless rims; I = igneous zircon: dark concentric oscillatory-zoned cores or single grains. Other symbols see table 2.

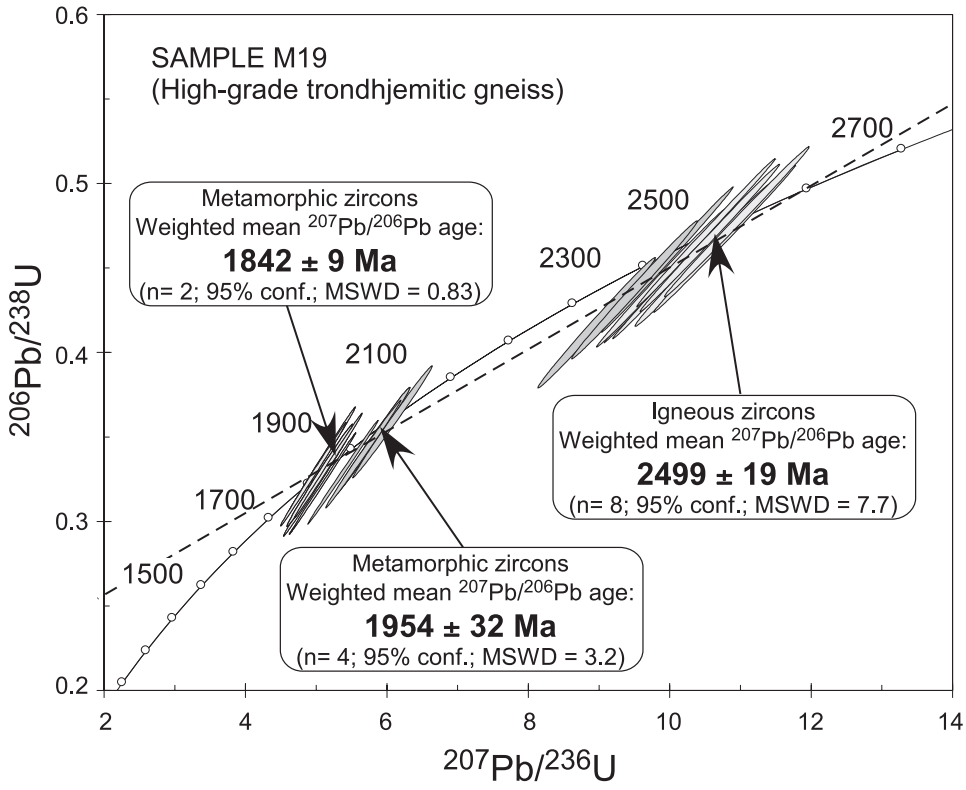

Fig. 8. Concordia plot of SHRIMP U-Pb zircon analytical results for the Huai'an trondhjemitic gneiss (sample M19). Errors as in figure 7.

and bright (high luminescence) structureless rims (fig. 6F). The dark zoned cores are interpreted to be of igneous origin, whereas the bright, structureless rims are considered to have resulted from metamorphic recrystallization or overgrowth. Table 5 lists ten analyses for sample M17, of which two were made on individual metamorphic zircon grains, four on magmatic zircon cores with oscillatory zoning, and four on bright (high luminescence), structureless, metamorphic rims. On a concordia plot (fig. 10), the metamorphic zircons form a nearly concordant group that gives a weighted mean $^{207}Pb/^{206}Pb$ age of 1848 ± 19 Ma (MSWD = 0.13), interpreted as approximating the peak of the metamorphic event. This age is comparable to the somewhat more precise ages obtained from the Huai'an TTG gneiss samples. Of the four analyses on dark (highly luminescent) oscillatorily-zoned zircon cores, one analysis is concordant, giving a $^{207}Pb/^{206}Pb$ age of 1964 ± 60 Ma, with a large error, which is comparable to the emplacement age (~1915 Ma) of the metamorphosed mafic dike swarm in the Hengshan Complex (Kröner and others, 2006), 50 km south of the Huai'an Complex. The remaining three analyses are variably discordant, giving $^{207}Pb/^{206}Pb$ ages of 2032 ± 86 Ma, 2040 ± 39 Ma and 2201 ± 68 Ma (fig. 10), which may represent the crystallization ages of xenocrystic zircons entrained in the mafic protolith.

Dongjiagou granitic gneiss (sample M28).—Most zircons in sample M28 are euhedral to subhedral prisms with sharp terminations, evidently of igneous origin, which is further supported by their CL images revealing oscillatory zoning. Some zircons have an oscillatory-zoned core with a bright, structureless rim (fig. 5G). Like those in other

TABLE 4

U-Th-Pb SHRIMP data for sample M23 (granodioritic gneiss)

Spot	Texture	ppm U	ppm Th	$^{232}Th/^{238}U$	ppm $^{206}Pb^*$	$^{204}Pb/^{206}Pb$	% $^{206}Pb_c$	$^{207}Pb^*/^{206}Pb^*$	±%	$^{207}Pb^*/^{235}U$	±%	$^{206}Pb^*/^{238}U$	±%	err corr	% conc	$^{207}Pb^*/^{206}Pb^*$ age	
M23-1	M	322	129	0.41	0.34	2.1E-4	0.33	.1127	0.8	4.95	2.5	.3187	2.4	.947	97	1843	±14
M23-2	M	104	34	0.33	1.21	7.6E-4	1.18	.1092	2.1	4.68	3.3	.3107	2.5	.758	98	1785	±39
M23-3	M	291	166	0.59	0.18	1.1E-4	0.17	.1132	0.7	4.95	2.5	.3168	2.4	.955	96	1852	±13
M23-4	I	84	34	0.41	-0.01	5.1E-6	--	.1569	1.8	9.45	3.2	.4371	2.6	.828	97	2422	±30
M23-5	M	55	59	1.10	0.42	2.6E-4	0.41	.1124	1.7	5.07	3.2	.3275	2.6	.835	99	1838	±32
M23-6	M	247	91	0.38	0.20	1.2E-4	0.19	.1141	0.8	5.30	2.5	.3372	2.4	.946	100	1865	±15
M23-7	I	199	41	0.21	0.06	4.0E-5	0.06	.1600	0.6	10.59	2.4	.4798	2.4	.973	103	2456	±10
M23-9	I	193	29	0.16	0.26	1.6E-4	0.23	.1553	0.8	9.51	2.5	.4442	2.4	.949	99	2405	±13
M23-10	M	551	157	0.29	0.10	6.5E-5	0.10	.1128	0.5	5.24	2.4	.3367	2.3	.980	101	1845	±9
M23-11	I	55	19	0.36	0.12	7.2E-5	0.10	.1616	1.4	9.60	2.9	.4310	2.5	.870	93	2472	±24
M23-12	I	198	65	0.34	0.00	1.5E-6	--	.1611	1.2	9.68	2.7	.4357	2.4	.899	94	2468	±20
M23-13	I	17	6	0.37	0.53	3.3E-4	0.48	.1567	1.8	9.58	3.4	.4435	2.9	.857	98	2420	±30
M23-14	I	48	15	0.32	0.41	2.6E-4	0.37	.1550	1.5	9.10	2.9	.4259	2.5	.856	95	2401	±26
M23-15	I	106	49	0.47	0.00	6.3E-8	0.00	.1724	0.6	11.21	2.5	.4715	2.4	.971	96	2581	±10
M23-16	M	96	7	0.07	0.11	7.2E-5	0.11	.1109	1.3	4.95	2.7	.3236	2.4	.879	100	1814	±24
M23-17	M	111	8	0.07	0.22	1.4E-4	0.22	.1138	1.1	5.24	2.6	.3341	2.4	.911	100	1862	±20

*Texture: I = igneous zircon; M = metamorphic zircon. Other symbols see table 2.

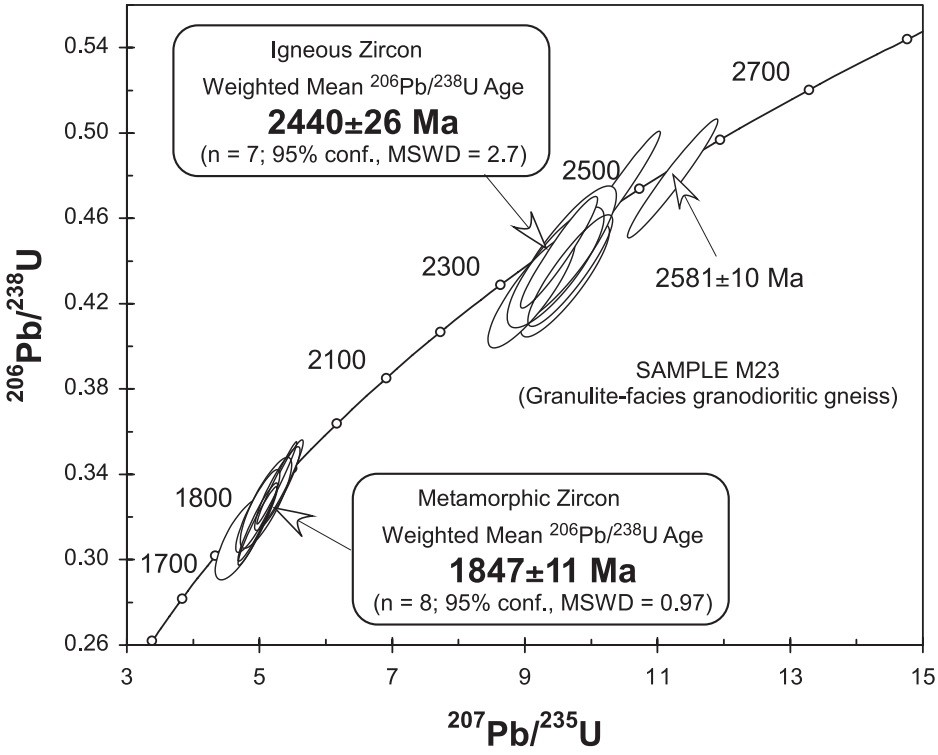

Fig. 9. Concordia plot of SHRIMP U-Pb zircon analytical results for the Huai'an granodioritic gneiss (sample M23). Errors as in figure 7.

samples, the narrow structureless rims with high luminescence are interpreted to be the result of metamorphic recrystallization or overgrowth, whereas the dark oscillatory-zoned cores are of igneous origin. The analytical data are presented in table 6 and on a concordia plot in figure 11. Of 14 analyses, ten were made on oscillatory-zoned igneous zircons (with or without metamorphic rims), and four were made on highly luminescent and structureless metamorphic rims. All analyses of igneous zircons (fig. 11) form a concordant group with a weighted mean $^{207}Pb/^{206}Pb$ age of 2036 ± 16 Ma (MSWD = 2.2), interpreted as the crystallization age of the gneiss protolith. The four analyses on the metamorphic rims are also nearly concordant and give a weighted mean $^{207}Pb/^{206}Pb$ age of 1839 ± 46 Ma, interpreted as the approximate age of the metamorphic event. Despite the large error and high MSWD, this age is comparable to those obtained from metamorphic zircons in all samples previously described in this paper.

Huai'an charnockite (Sample M22).—Sample M22 was collected from a massive charnockite body that locally intrudes the high-grade tonalitic gneiss (fig. 3). Zircons in sample M22 form a homogeneous population of euhedral prisms. The internal structures as revealed by CL images are characterized by irregular zoning (fig. 5H) without structureless rims. The analytical data are presented in table 7 and on a concordia plot in figure 12. Sixteen out of 18 analyses are concordant, or nearly concordant, and yielded a weighted mean $^{207}Pb/^{206}Pb$ age of 1849 ± 10 Ma (fig. 12), interpreted as the crystallization age of the Huai'an charnockite. Two analyses are discordant (spots 14 and 18), possibly due to their high U-contents, but relatively strongly correlated with the other data points, and a regression through all 18 data-points, using the program IsoplotEx, defines a chord with an upper concordia

TABLE 5

U-Th-Pb SHRIMP data for sample M17 (Manjinggou HPgranulite)

Spot	Texture	ppm U	ppm Th	$^{232}Th/^{238}U$	ppm $^{206}Pb^*$	$^{204}Pb/^{206}Pb$	% $^{206}Pb_c$	$^{207}Pb^*/^{206}Pb^*$	±%	$^{207}Pb^*/^{235}U$	±%	$^{206}Pb^*/^{238}U$	±%	err corr	% conc	$^{207}Pb^*/^{206}Pb^*$ age	
M17-1	M	25	11	0.46	6.68	2.5E-4	0.38	0.1128	3.3	4.75	4.1	0.3055	2.5	.597	93	1844	± 60
M17-2	I	38	11	0.29	11.1	3.2E-4	0.49	0.1258	2.2	5.91	3.2	0.3406	2.3	.717	93	2040	± 39
M17-3	M	39	19	0.52	10.8	5.3E-4	0.83	0.1125	2.7	4.99	3.5	0.3217	2.2	.636	98	1841	± 48
M17-4	M	36	5	0.15	9.79	6.3E-4	0.98	0.1122	3.5	4.81	4.1	0.3111	2.2	.542	95	1835	± 63
M17-5	M	14	4	0.29	3.71	2.5E-4	0.39	0.1155	3.1	5.01	4.1	0.3144	2.7	.662	93	1888	± 55
M17-6	I	10	2	0.22	2.85	3.2E-4	0.48	0.1252	4.8	5.89	5.7	0.341	3.1	.538	93	2032	± 85
M17-7	M	13	2	0.19	4.17	1.2E-3	1.74	0.1146	5.9	5.81	6.6	0.368	2.8	.431	108	1874	±110
M17-8	I	27	6	0.22	8.05	2.0E-4	--	0.1205	3.3	5.83	4.1	0.3509	2.3	.568	99	1964	± 60
M17-9	I	19	7	0.36	6.16	5.5E-4	0.83	0.1379	3.9	7.08	4.7	0.3723	2.5	.544	93	2201	± 68
M17-10	M	250	121	0.50	70.0	5.9E-5	0.09	0.11295	0.58	5.078	1.9	0.3260	1.8	.953	98	1847	± 10

Texture: M = metamorphic zircon: bright (high luminescence) near-spherical and structureless single grains or structureless rims; I = igneous zircon: dark (low luminescence) oscillatorily-zoned cores. Other symbols see table 2.

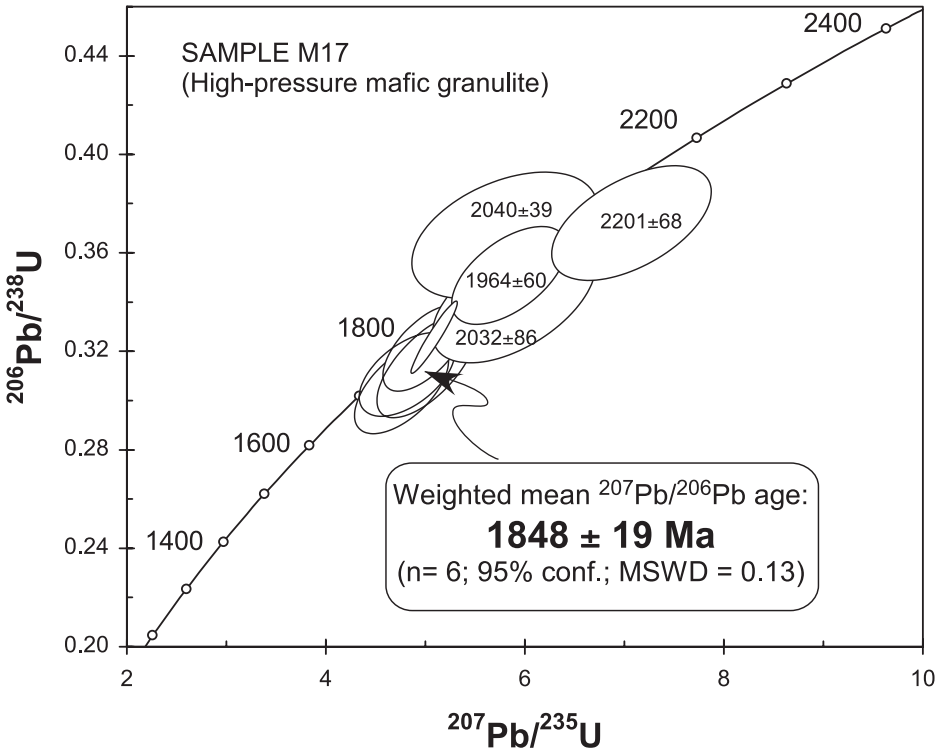

Fig. 10. Concordia plot of SHRIMP U-Pb zircon analytical results for the Manjinggou high-pressure mafic granulite (sample M17). Errors as in figure 7.

intercept age of 1847 ± 15 Ma (MSWD = 0.86), identical to the weighted mean $^{207}Pb/^{206}Pb$ age defined by the 16 concordant data points. The crystallization age of the massive charnockite is identical to the metamorphic ages obtained from the Huai'an TTG gneisses, which supports the conclusion that the charnockite formed by anatexis of the gneisses during the peak of high-grade metamorphism (Liu, ms, 1995).

Dapinggou garnet-bearing S-type granite (Sample M24).—Sample M24 was collected in the southwestern part of the Manjinggou area (fig. 3). CL images of all zircons are characterized by concentric oscillatory zoning (fig. 5I), without overgrowth rims, evidently of igneous origin. The analytical data are presented in table 8 and on a concordia plot in figure 13. The eight analyses are concordant to nearly concordant and yielded a weighted wean $^{207}Pb/^{206}Pb$ age of 1850 ± 17 Ma (MSWD = 1.3) (fig. 13), interpreted as the crystallization age of the granite. This age is identical to the ages of metamorphic zircons from other lithologies in the Huai'an Complex, supporting the previous conclusion (Lu, 1991; Lu and Jin, 1993) that the Dapinggou granite is a syn-tectonic intrusion that was derived by anatexis of Al-rich gneisses of the Khondalite Series.

DISCUSSION AND IMPLICATIONS

Table 9 summarizes our new zircon data, which, when combined with data from other complexes in the TNCO (for example, Hengshan, Wutai, Fuping and Xuanhua Complexes), enable us to place constraints on several key issues related to the late Archean to Paleoproterozoic accretion and evolution of the orogen.

TABLE 6

U-Th-Pb SHRIMP data for sample M28 (Dongjiagou granitic gneiss)

Spot	Texture	ppm U	ppm Th	$^{232}Th/^{238}U$	ppm $^{206}Pb^*$	$^{204}Pb/^{206}Pb$	% $^{206}Pb_c$	$^{207}Pb^*/^{206}Pb^*$	±%	$^{207}Pb^*/^{235}U$	±%	$^{206}Pb^*/^{238}U$	±%	err corr	% conc	$^{207}Pb^*/^{206}Pb^*$ age	
M28-1	M	125	6	0.05	35.6	1.8E-4	0.28	0.1107	1.2	5.04	2.7	0.3302	2.4	.896	102	1811	±22
M28-2	I	200	106	0.55	66.6	2.3E-5	0.03	0.1275	0.79	6.82	2.5	0.3881	2.4	.950	102	2064	±14
M28-3	M	505	19	0.04	146	7.8E-5	0.12	0.1146	0.51	5.31	2.4	0.3358	2.3	.977	100	1873	± 9.2
M28-4	I	206	99	0.49	67.6	3.2E-5	0.05	0.1261	0.71	6.63	2.5	0.3812	2.4	.958	102	2044	±13
M28-5	I	131	73	0.57	43.0	1.3E-4	0.19	0.1248	0.93	6.55	2.6	0.3807	2.4	.934	103	2026	±16
M28-6	I	234	29	0.13	77.4	9.1E-5	0.14	0.1276	1.6	6.75	2.9	0.3836	2.4	.835	101	2065	±28
M28-7	I	317	415	1.35	103	1.7E-4	0.26	0.1252	0.88	6.55	2.5	0.3790	2.4	.937	102	2032	±15
M28-8	I	132	83	0.65	42.7	5.1E-6	--	0.1263	0.85	6.56	2.6	0.3764	2.4	.944	101	2047	±15
M28-9	M	633	88	0.14	181	2.2E-5	0.03	0.1112	0.41	5.10	2.4	0.3326	2.4	.985	102	1819	± 7.5
28-10	I	206	215	1.08	66.0	1.3E-4	0.20	0.1228	0.76	6.29	2.5	0.3718	2.4	.953	102	1997	±13
M28-11	I	151	72	0.50	51.0	2.1E-5	0.03	0.1274	0.94	6.93	2.6	0.3945	2.4	.931	104	2062	±17
M28-12	I	183	79	0.45	58.9	3.8E-5	--	0.1256	0.93	6.50	2.6	0.3751	2.4	.932	101	2038	±16
M28-13	M	150	5	0.04	43.7	6.6E-5	0.10	0.1124	0.93	5.25	2.6	0.3387	2.4	.933	102	1838	±17
M28-14	I	160	137	0.89	53.4	1.2E-4	0.18	0.1239	0.82	6.63	2.5	0.3881	2.4	.947	105	2014	±15

*Texture: M = metamorphic zircon; I = igneous zircon. Other symbols see table 2.

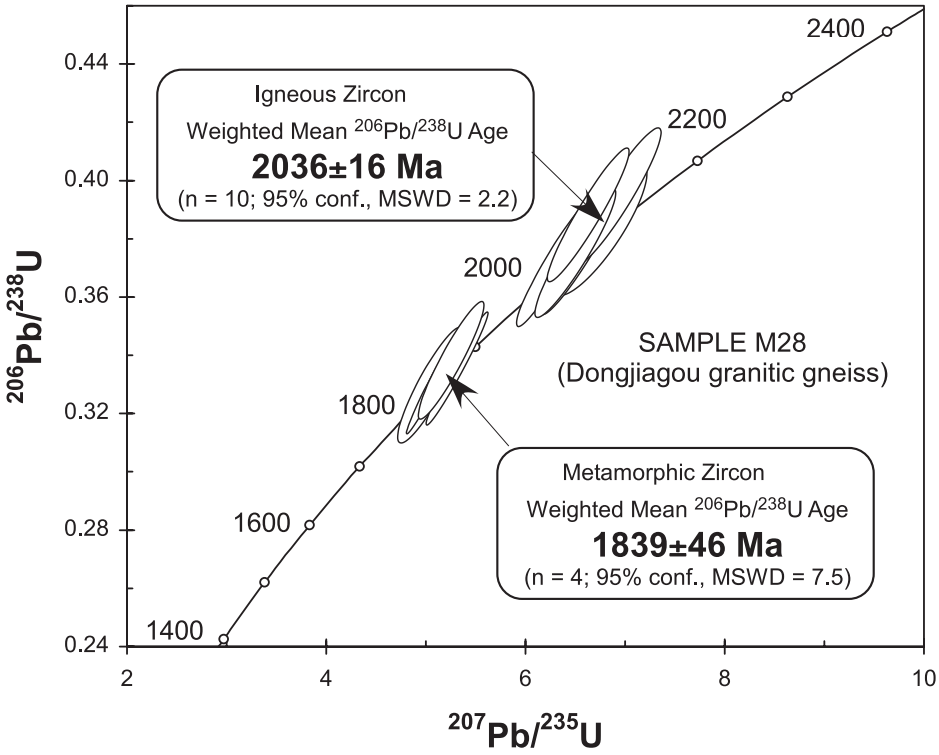

Fig. 11. Concordia plot of SHRIMP U-Pb zircon analytical results for the Dongjiagou granitic gneiss (sample M28). Errors as in figure 7.

Emplacement of high-grade TTG gneisses and their relationship to low-grade granite-greenstone associations.—One of the key issues in the late Archean to Paleoproterozoic accretion and evolution of the TNCO is the temporal relationship between the high-grade TTG gneisses and low-grade granite-greenstone associations. The high-grade gneisses make up over 60 percent of the total exposure of the TNCO and are mainly exposed in the Fuping, Hengshan, Huai'an, Xuanhua and Taihua Complexes, whereas the low-grade granite-greenstone associations are dominant in the Wutai, Zhongtiao, Zanhuang, Dengfeng and Northern Hebei Complexes (fig. 1). It has long been considered that the high-grade gneisses constitute an older continental basement to the low-grade granite-greenstone associations (Bai, 1986; Ma and others, 1987; Li and others, 1990; Tian, 1991; Bai and others, 1992; Wang and others, 1996; Bai and Dai, 1998; Polat and others, 2005). This model was mainly based on conventional multigrain U–Pb zircon and whole-rock Sm-Nd isochron ages, which suggested that the TTG gneisses in the TNCO were emplaced in the period between 2800 and 2560 Ma (Liu and others, 1985; Bai, 1986; Wu and others, 1989; Tian, 1991). However, recent SHRIMP U-Pb zircon data convincingly demonstrate that both granitoids and volcanics in the low-grade granite-greenstone terranes formed at the same time, or slightly earlier, as emplacement of the precursors to the high-grade TTG gneisses. For example, the granitoids and greenstone-type volcanics in the low-grade Wutai and Zhongtiao complexes crystallized at 2560 to 2520 Ma and 2530 to 2515 Ma, respectively, whereas the protoliths of the high-grade Hengshan, Fuping and Xuanhua gneisses were emplaced in the period 2520 to 2480 Ma (see table 10, also for related

TABLE 7

U-Th-Pb SHRIMP data for sample M22 (Huai'an charnockite)

Spot	ppm U	ppm Th	$^{232}Th/^{238}U$	ppm $^{206}Pb^*$	$^{204}Pb/^{206}Pb$	% $^{206}Pb_c$	$^{207}Pb^*/^{206}Pb^*$	±%	$^{207}Pb^*/^{235}U$	±%	$^{206}Pb^*/^{238}U$	±%	err corr	% conc.	$^{207}Pb^*/^{206}Pb^*$ age	
M22-1	614	38	0.06	175	1.8E-5	0.03	0.1127	0.36	5.15	2.3	0.3314	2.3	.988	100	1843	±6.5
M22-2	433	13	0.03	125	1.3E-5	0.02	0.1132	0.39	5.26	2.3	0.3370	2.3	.986	101	1851	±7.0
M22-3	336	11	0.03	98.0	4.4E-4	0.68	0.1149	0.91	5.35	2.5	0.3374	2.3	.929	100	1879	±16
M22-4	205	5	0.03	58.0	6.8E-5	0.11	0.1114	0.70	5.06	2.4	0.3296	2.3	.956	101	1822	±13
M22-5	737	23	0.03	202	3.9E-5	0.06	0.1107	0.56	4.86	2.3	0.3185	2.3	.970	98	1811	±10
M22-6	381	6	0.02	107	4.2E-6	--	0.1127	0.41	5.09	2.3	0.3276	2.3	.984	99	1844	±7.5
M22-7	611	28	0.05	175	2.5E-5	0.04	0.1131	0.80	5.20	2.4	0.3335	2.3	.944	100	1850	±15
M22-8	616	14	0.02	178	1.6E-5	0.02	0.1131	0.42	5.24	2.3	0.3363	2.3	.984	101	1849	±7.5
M22-9	274	6	0.02	78.7	2.9E-5	--	0.1143	0.51	5.28	2.5	0.3348	2.4	.978	100	1869	±9.3
M22-10	720	30	0.04	209	1.8E-5	0.03	0.1138	0.30	5.30	2.3	0.3379	2.3	.991	101	1860	±5.5
M22-11	462	12	0.03	131	9.3E-5	0.14	0.1137	0.44	5.18	2.3	0.3306	2.3	.982	99	1859	±7.9
M22-12	758	17	0.02	216	6.3E-5	0.10	0.1138	0.45	5.20	2.3	0.3311	2.3	.981	99	1861	±8.1
M22-13	432	21	0.05	120	5.0E-5	0.08	0.1102	0.44	4.90	2.3	0.3227	2.3	.982	100	1802	±8.0
M22-14	1098	24	0.02	237	2.2E-4	0.35	0.1016	1.3	3.505	2.8	0.2502	2.5	.887	87	1654	±24
M22-15	960	18	0.02	286	1.5E-5	0.02	0.1132	0.31	5.41	2.3	0.3466	2.3	.991	104	1852	±5.5
M22-16	499	15	0.03	142	3.4E-5	0.05	0.1142	0.38	5.23	2.3	0.3320	2.3	.986	99	1867	±6.8
M22-17	107	4	0.04	30.9	1.3E-4	0.21	0.1113	1.2	5.16	2.6	0.3360	2.3	.894	103	1821	±21
M22-18	1216	23	0.02	285	6.4E-5	0.10	0.1032	1.1	3.88	2.6	0.2726	2.4	.912	92	1682	±20

Errors are 1-sigma; Pb_c and Pb* indicate the common and radiogenic portions, respectively. Common Pb corrected using measured ^{204}Pb.

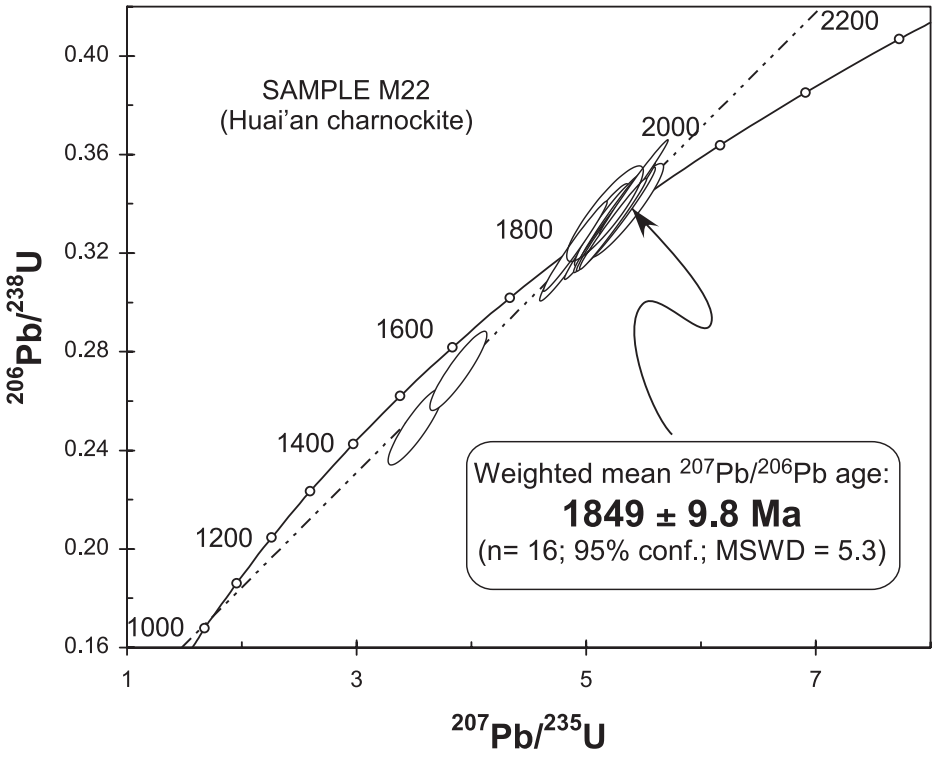

Fig. 12. Concordia plot of SHRIMP U-Pb zircon analytical results for the Huai'an charnockite (sample M22). Errors as in figure 7.

references). Similarly, SHRIMP zircon ages presented in this study for the Huai'an TTG gneisses do not support the model that the high-grade gneiss complexes constitute a basement to the low-grade granite-greenstone terranes. These data show that the first major igneous phase in the Huai'an complex was the emplacement of tonalites at 2515 ± 20 Ma, followed by trondhjemites at 2499 ± 19 Ma and ranodiorites at 2440 ± 26 Ma. Therefore, TTG magmatism in the TNCO occurred over a protracted interval from the late Archean (~2520 Ma) to early Paleoproterozoic (~2440 Ma). This supports our earlier suggestion that the high-grade TTG gneiss complexes and low-grade granite-greenstone terranes constitute a single late Archean to Paleoproterozoic magmatic arc system where the low-grade granite-greenstone associations (for example, Wutai and Zhongtiao complexes) represent upper crustal, calc-alkaline volcano-plutonic assemblages, whereas the high-grade TTG gneisses represent the lower crustal components forming the root of the arc (Zhao and others, 2007, and references therein).

Paleoproterozoic pre-tectonic granitoid magmatism.—In the older Chinese literature, much of the lithologies in the TNCO was considered to have formed during late Archean time. However, recent SHRIMP zircon ages reveal the widespread existence of deformed and metamorphosed Paleoproterozoic granitoids. For example, the Lüliang complex (see fig. 1) does not contain Archean rocks but consists exclusively of Paleoproterozoic granitoids and volcano-sedimentary rocks metamorphosed from greenschist- to amphibolite-facies, of which the granitoid gneisses yielded SHRIMP zircon ages ranging from 2375 ± 10 Ma to 2173 ± 7 Ma (Zhao and others, 2008). In the

TABLE 8

U-Th-Pb SHRIMP data for sample M24 (Dongjiagou garnet-bearing S-type granite)

Spot	ppm U	ppm Th	$^{232}Th/^{238}U$	ppm $^{206}Pb^*$	$^{204}Pb/^{206}Pb$	% $^{206}Pb_c$	$^{207}Pb^*/^{206}Pb^*$	±%	$^{207}Pb^*/^{235}U$	±%	$^{206}Pb^*/^{238}U$	±%	err corr	% conc.	$^{207}Pb^*/^{206}Pb^*$ age	
M24-1	265	16	0.06	74.9	9.3E-5	0.14	0.1123	0.54	5.082	1.4	0.3282	1.3	.927	100	1837	± 9.9
M24-2	167	7	0.04	46.9	1.1E-4	0.17	0.1130	0.72	5.101	1.6	0.3273	1.4	.885	99	1849	± 13
M24-3	267	14	0.05	75.9	9.7E-5	0.15	0.1149	0.81	5.220	1.6	0.3297	1.3	.856	98	1877	± 15
M24-5	177	6	0.04	51.4	5.3E-4	0.82	0.1126	2.3	5.20	2.6	0.3353	1.4	.520	101	1841	± 41
M24-6	244	9	0.04	71.7	5.6E-4	0.86	0.1135	2.3	5.29	2.7	0.3382	1.4	.509	101	1857	± 42
M24-7	257	13	0.05	75.1	3.7E-4	0.58	0.1148	1.1	5.348	1.8	0.3380	1.4	.794	100	1876	± 20
M24-8	149	5	0.04	43.3	6.7E-4	1.05	0.1102	1.7	5.09	2.2	0.3351	1.4	.638	103	1803	± 31
M24-9	170	11	0.07	46.4	7.1E-4	1.11	0.1127	2.7	4.90	3.0	0.3149	1.4	.459	96	1844	± 48

Errors are 1-sigma; Pb_c and Pb* indicate the common and radiogenic portions, respectively. Common Pb corrected using measured ^{204}Pb.

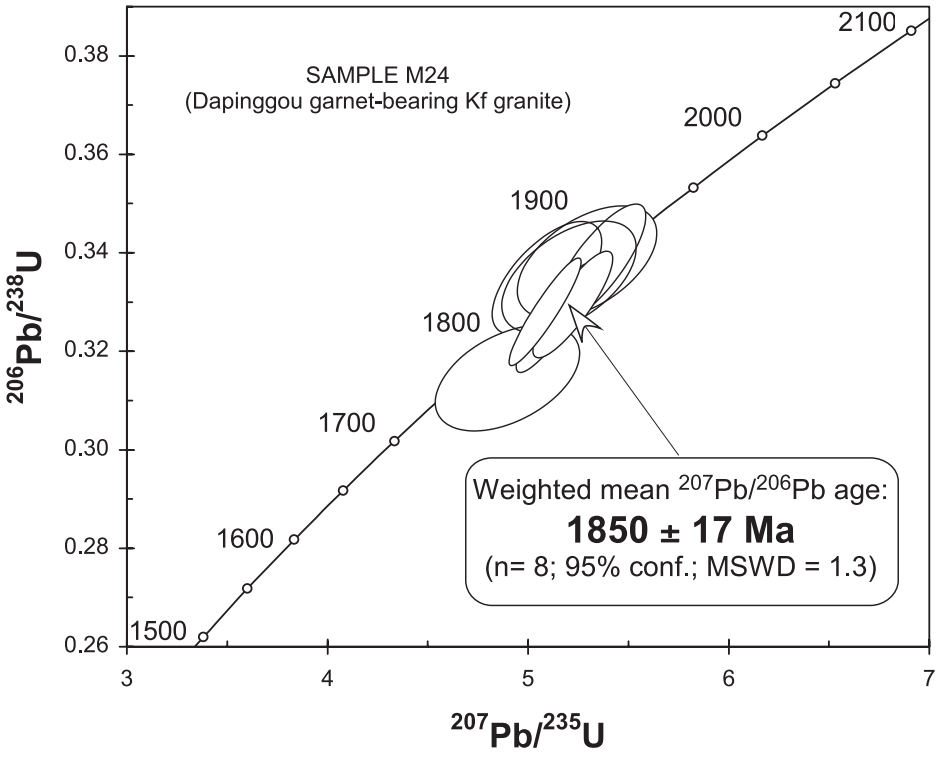

Fig. 13. Concordia plots of SHRIMP U-Pb zircon analytical results for the Dapinggou garnet-bearing S-type granite (sample M24). Errors as in figure 7.

Wutai complex, Paleoproterozoic granitoids are represented by the Dawaliang pluton and the pink phase of the Wangjiahui granite, of which the former yielded a SHRIMP zircon age of 2176 ± 12 Ma, whereas three samples of the latter were dated at 2117 ± 17 Ma, 2116 ± 16 Ma and 2084 ± 20 Ma, respectively (Wilde and others, 2005). In the Fuping Complex, Paleoproterozoic magmatism is represented by the Nanying granitoid gneisses, of which three samples yielded SHRIMP zircon ages of 2109 ± 5 Ma, 2097 ± 6 Ma, and 2097 ± 46 Ma (Zhao and others, 2002; Guan and others, 2002). In addition, Kröner and others (2005a, 2005b) recognized three phases of Paleoproterozoic gneissic granitoids in the Hengshan Complex that were emplaced at 2360 to 2330 Ma, ~2250 Ma and ~2110 Ma, respectively.

Above we report a SHRIMP zircon age of 2036 ± 16 Ma for the Dongjiagou gneiss from the Huai'an complex. This is nearly identical to the age of the Nanying gneisses in the Fuping Complex and the younger phase of granitoid gneisses in the Lüliang complex. These Paleoproterozoic gneisses contain the same deformational fabrics as the high-grade TTG gneisses and thus unambiguously demonstrate that the main deformational event in the TNCO is not Archean but Paleoproterozoic in age (see for example, Kröner and others, 2005a, 2005b). Geochemically, most Paleoprotrozoic granitoids in the TNCO have geochemical affinities to modern magmatic arcs (Geng and others, 2000; Zhao and others, 2002; Guan and others, 2002; Liu and others, 2005), similar to the TTG gneisses in the high-grade gneiss complexes. This suggests that most rocks in the TNCO represent elements of a long-lived magmatic arc, with the earliest arc-related plutonic event at 2560 to 2520 Ma, marked by the emplacement of

TABLE 9

Summary of SHRIMP zircon ages for major lithologies of the Huai'an Complex

Samples Number	Rock type	Magmatic crystallization age	Metamorphic age	Ages of inherited or xenocrystic zircons
M21	Tonalitic gneiss (Huai'an TTG gneisses)	**2515±20 Ma** (MSWD = 5.5) (a weighted $^{207}Pb/^{206}Pb$ age for 7 analyses on magmatic zircons)	**1847±17 Ma** (MSWD = 3.8) (a weighted $^{207}Pb/^{206}Pb$ age for 7 analyses on metamorphic zircons)	
M19	Trondhjemitic gneiss (Huai'an TTG gneisses)	**2499±19 Ma** (MSWD = 7.7) (a weighted $^{207}Pb/^{206}Pb$ age for 7 analyses on magmatic zircons)	**1842±10 Ma** (MSWD = 0.83) (a weighted $^{207}Pb/^{206}Pb$ age from 2 analyses on metamorphic zircons)	
M23	Granodoritic gneiss (Huai'an TTG gneisses)	**2440±26 Ma** (MSWD = 2.7) (a weighted $^{207}Pb/^{206}Pb$ age for 7 analyses on magmatic zircons)	**1847 ± 11 Ma** (MSWD = 0.97) (a weighted $^{207}Pb/^{206}Pb$ age from 7 analyses on metamorphic zircons)	2581±10 Ma
M17	Manjinggou mafic high-pressure granulite	**1964±60 Ma** (?)	**1848 ± 19 Ma** (MSWD = 0.13) (a weighted $^{207}Pb/^{206}Pb$ age from 6 analyses on metamorphic zircons)	2032±86 Ma 2040±39 Ma 2201±68 Ma
M28	Dongjiagou granitic gneiss	**2036±16 Ma** (MSWD = 2.2) (a weighted $^{207}Pb/^{206}Pb$ age for 10 analyses on magmatic zircons)	**1839 ± 46 Ma** (MSWD = 7.5) (a weighted $^{207}Pb/^{206}Pb$ age from 4 analyses on metamorphic zircons)	
M22	Huai'an charnockite	**1849±9.8 Ma** (MSWD = 5.3) (a weighted $^{207}Pb/^{206}Pb$ age for 16 analyses on magmatic zircons) **1847±15 Ma (MSWD=0.86)** (Upper intercept age for 18 analyses)	**1849±10 Ma**	2053±7 Ma
M24	Dapinggou garnet-bearing S-type granite	**1850±17 Ma** (MSWD = 1.3) (a weighted $^{207}Pb/^{206}Pb$ age for 8 analyses on magmatic zircons)	**1850±17 Ma**	

granitoids into older granitic basement at a continental margin, represented by the western margin of the Eastern Block of the North China Craton. These were later tectonically interleaved with the low-grade granite-greenstone terrane that records arc volcanism at 2530 to 2515 Ma. This upper crustal volcanism overlapped with the lower crustal emplacement of the TTG suite precursors in the high-grade gneiss complexes

TABLE 10

Summary of SHRIMP U-Pb zircon ages for low-grade granites and greenstones and high-grade TTG gneisses in the Trans-North China Orogen

Sample	Description	Age (Ma)	Sources
Granitoids in low-grade granite-greenstone terranes (2560-2520 Ma)			
Ekou Granite			
95-PC-34	Deformed granitoid	2566±13	Wilde and others (1997)
95-19	Deformed granitoid	2555±6	Wilde and others (1997)
Chechang-Beitai Granite			
WC7	Foliated tonalite	2552±11	Wilde and others (1997)
95-PC-6B	Foliated tonalite	2551±5	Wilde and others (1997)
WC6	Deformed granodiorite	2546±6	Wilde and others (1997)
WC5	Deformed granodiorite	2538±6	Wilde and others (1997)
Lanzhishan Granite			
95-PC-94	Deformed granitoid	2553±8	Wilde and others (1997)
95-PC-96	Deformed granitoid	2537±10	Wilde and others (1997)
Shifo Pluton			
95-PC-98	Deformed monzogranite	2531±4	Wilde and others (2005)
Guangmishi Granite			
95-PC-76	Deformed granitoid	2531±5	Wilde and others (2005)
Wangjiahui Granite (Grey Phase)			
95-PC-62	Deformed granodiorite	2520±9	Wilde and others (2005)
95-PC-63	Deformed granodiorite	2517±12	Wilde and others (2005)
Longquanguan augen gneisses			
WL12	Sheared porphyritic granitoid	2543±7	Wilde and others (2005)
WN11	Sheared tonaltic granitoid	2541±14	Wilde and others (2005)
WL9	Sheared porphyritic granitoid	2540±18	Wilde and others (2005)
Sushui pluton			
ZT4020-1	Foliated trondhjemite	2553±14	Tian and others (2005)
2530-2515 Ma greenstones in low-grade granite-greenstone terranes			
95PC-114	Meta-andesite, Zhuangwang "Formation"	2529±10	Wilde and others (2004b)
96PC-119	Meta-andesite, Zhuangwang "Formation"	2513±8	Wilde and others (2004b)
95-PC-115	Meta-andesite, Baizhiyan "Formation"	2524±10	Wilde and others (2004b)
WT13	Meta-rhyolite, Hongmenyan "Formation"	2533±8	Wilde and others (2004b)
WT17	Meta-rhyodacite Hongmenyan "Formation"	2524±8	Wilde and others (2004b)
WT9	Meta-dacite, Hongmenyan "Formation"	2523±9	Wilde and others (2004b)
WT12	Meta-rhyodacite, Hongmenyan "Formation"	2516±10	Wilde and others (2004b)
95-PC-55c	Meta-rhyolite, Gaofan "Subgroup" (Xiazhuang)	2528±6	Wilde and others (2004b)
2520-2440 Ma TTG gneisses in high-grade gneiss complexes			
Hengshan TTG gneisses			
980814	Dioritic gneiss	2479±3	Kröner and others (2005b)
990803	Dioritic gneiss with melt patches	2475±2	Kröner and others (2005b)
990859	Dioritic gneiss	2506±5	Kröner and others (2005b)
HG1	Tonalitic gneiss	2520±15	Kröner and others (2005b)
HG5	Trondhjemitic gneiss	2520±10	Kröner and others (2005b)
HG6	Trondhjemitic gneiss	2526±12	Kröner and others (2005b)
HG7	Trondhjemitic gneiss	2507±4	Kröner and others (2005b)

TABLE 10
(continued)

990847	Trondhjemitic gneiss	2524±8	Kröner and others (2005b)
980809	Foliated pegmatitic red gneiss	2501±3	Kröner and others (2005b)
990873	Foliated gneiss from migmatite	2499±6	Kröner and others (2005b)
990821	Finely layered biotite gneiss	2526±4.7	Kröner and others (2005b)
Yixingzhai TTG gneisses			
96PC153	Homogeneous tonalitic gneiss	2513±15	Wilde (2002)
96PC154	Quartz dioritic gneiss, a roadcut	2499±4	Wilde (2002)
Fuping TTG gneisses			
FG1	Layered tonalitic gneiss, a roadcut	2523±14	Zhao and others (2002)
FP50	Foliated, hornblende tonalitic gneiss	2520±20	Guan and others (2002)
FP54	Trondhjemitic gneiss	2513±12	Guan and others (2002)
FP217	Trondhjemitic gneiss	2499±9.5	Zhao and others (2002)
FP216	Granodioritic gneiss	2486 ± 8	Zhao and others (2002)
FP08	Granodioritic gneiss	2475±8	Guan and others (2002)
FP236	Mylonitized monzongranitic gneiss	2510±22	Zhao and others (2002)
FP224	Mylonitized pegmatitic dike	2507±11	Zhao and others (2002)
Xuanhua TTG gneisses			
Z9116	Granodioritic gneiss	2515±7	Liu and Geng (1997)
Huai'an TTG gneisses			
M21	Tonalitic gneiss	2515±20	This study
M19	Trondhjemitic gneiss	2499±19	This study
M23	Granodioritic gneiss	2440±26	This study

at 2520 to 2440 Ma. Sporadic phases of Paleoproterozoic granitoid magmatism occurred in the period 2360 to 2000 Ma. Such long-lived magmatic arcs have also been documented in other Precambrian orogenic belts, including the 1.8 to 1.3 Ga magmatic arcs in southeastern Laurentia (Rivers and Corrigan, 2000; Kalstrom and others, 2001), southern Baltica (Bingen and others, 2002), central Australia (Giles and others, 2002), and western Amazonia (Geraldes and others, 2001). A present-day example of a long-lived magmatic arc is the Andes, where the Pacific plate has been subducting under the west coast of South America for ~500 million years (Dalziel, 1997). These examples demonstrate that a long-lived continental-margin arc is not unique to the TNCO.

Timing of the collision between the Eastern and Western Blocks.—As mentioned earlier, controversy remains about the timing of this collision. Some workers propose that the collision occurred at ~2.5 Ga (Li and others, 2000; Kusky and Li, 2003; Kusky and others, 2007; Li and Kusky, 2007), whereas others believe that the final amalgamation of the two blocks was completed by ~1.85 Ga (Zhao and others, 1998, 1999c, 2001a, 2005; Zhao, 2001; Wilde and others, 2002; Guo and others, 2005; Kröner and others, 2005a, 2006; Liu and others, 2006). So far, advocates of the ~2.5 Ga collision model for the TNCO have not provided convincing isotopic data indicating that the orogen underwent high-grade metamorphism and intense ductile deformation at ~2.5 Ga. In contrast, numerous metamorphic ages obtained from nearly all metamorphic complexes in the TNCO support the ~1.85 Ga collision model (table 11). Metamorphic zircons from both the late Archean and Paleoproterozoic gneisses yield similar concordant $^{207}Pb/^{206}Pb$ ages in the range 1880 to 1820 Ma (table 11), which are 700 Ma to 150 Ma younger than their corresponding magmatic zircon cores. Metamorphic zircons in the 2515 to 2540 Ma Huai'an gneisses yielded metamorphic zircon ages of 1847 ± 17 Ma (tonalitic gneiss), 1842 ± 10 Ma (trondhjemitic gneiss) and 1847 ± 11

TABLE 11

Summary of metamorphic ages from the Trans-North China Orogen (1880–1800 Ma)

Sample	Description	Age (Ma)	Methods	Source
Fuping Complex				
FG1	Zircons from a tonalitic gneiss	1802±43	SHRIMP	(1)
FP217	Zircons from a trondhjemitic gneiss	1875±43	SHRIMP	(1)
FP216	Zircons from granodioritic gneiss	1825±12	SHRIMP	(1)
FP188-2	Zircons from a Nanying gneiss	1826±12	SHRIMP	(1)
FP204	Zircons from a Nanying gneiss	1850±9.6	SHRIMP	(1)
FP30	Two zircon rims from a gneissic granite	1825±18	SHRIMP	(2)
FP08	Zircons from a granodioritic gneiss	1817±26	SHRIMP	(2)
Zanhuang Complex				
99JX-91	Biotite from a mylonitic gneiss	1826±0.8	Ar/Ar	(3)
Wutai Complex				
unknown	Garnet amphibolite (Jingangku Formation)	1851±9	Sm-Nd	(4)
S2010-2-1	Monazites from a kyanite schist	1822±14	EPMA	(5)
S2010-2-1	Menonazites from a kyanite schist	1833±8	EPMA	(5)
SZ10	Meta-monazites from a kyanite schist	1847±62	EPMA	(5)
Hengshan Complex				
990803	One euhedral zircon from a dioritic gneiss	1881±8	SHRIMP	(6)
M068	Zircons from HP granulite	1850±3	SHRIMP	(7)
HG2	Zircons from HP granulite	1867±23	SHRIMP	(7)
Ch990839	Coarse-grained pegmatitic melt	1851±5	SHRIMP	(7)
HG1	Zircons from a granitic gneiss	1872±17	SHRIMP	(7)
Ch980871	Zircons from a retro-eclogite	1881±0.4	EVAP	(7)
Ch990853	Zircons from a retrograded eclogite	1859.7±0.5	EVAP	(7)
Ch990886	Zircons from a mafic granulite	1850.9±0.4	EVAP	(7)
Ch990848	Zircons from HP granulite	1885.6±0.4	EVAP	(7)
Taihua Complex				
TW0006/1	Graphite-garnet-sillimanite gneiss	1844±66	SHRIMP	(8)
TWJ358/1	Garnet-bearing gneissic granite	1871±14	SHRIMP	(8)
Huai'an Complex				
MQ91-8	Garnet-whole rock for HP granulite	1813±23	Sm-Nd	(9)
MJ35	Zircons from HP granulites	1817±12	SHRIMP	(9)
MJ36	Zircons from HP granulites	1817±12	SHRIMP	(9)
M21	Zircons from a tonalitic gneiss	1847±17	SHRIMP	(10)
M19	Zircons from a trondhjemitic gneiss	1842±9.8	SHRIMP	(10)
M23	Zircons from a granodioritic gneiss	1847±11	SHRIMP	(10)
M17	Zircons from a HP mafic granulite	1848±19	SHRIMP	(10)
M28	Zircons from a granitic gneiss	1839±46	SHRIMP	(10)
M22	Igneous zircons from anatectic charnockite	1849±9.8	SHRIMP	(10)
M24	Meta-zircons from a S-type granite	1850±17	SHRIMP	(10)
Xuanhua Complex				
XW99-8	Garnet-whole rock for HP granulite	1842±38	Sm-Nd	(11)
WM99-7	Garnet-whole rock for HP granulite	1856±26	Sm-Nd	(11)
XW22	Zircons from HP granulites	1803±9	SHRIMP	(9)
	Zircons from the same sample	1872±16	SHRIMP	(9)
XW23	Zircons from HP granulites	1819±16	SHRIMP	(9)
Chengde Complex				
By98020	Zircons from a HP granulite	1817±17	SGD	(12)

SHRIMP = Sensitive high-resolution ion microprobe; EVAP = Single grain evaporation; SGD = Single grain dissolution; EPMA = Electron Probe Microanalysis; Ar/Ar = mineral $^{40}Ar/^{39}Ar$; Meta-zircon = metamorphic zircons.

(1) = Zhao and others (2002); (2) = Guan and others (2002); (3) = Wang and others (2003); (4) = Wang and others (2001); (5) = Liu and others (2006); (6) = Kröner and others (2005a); (7) = Kröner and others (2005b); (8) = Wan and others (2006); (9) = Guo and others (2005); (10) = This study; (11) = Guo and Zhai (2001); (12) = Mao and others (1999).

Ma (granodioritic gneiss). Similarly, the 2036 ± 16 Ma Dongjiagou granitic yielded a metamorphic zircon age of 1839 ± 46 Ma, similar to that obtained from the 2520 to 2475 Ma Fuping gneisses and the 2050 to 2000 Ma Nanying gneisses in the Fuping

Complex (Zhao and others, 2002; Guan and others, 2002). We also obtained a metamorphic zircon age of 1848 ± 19 Ma for the Manjinggou high-pressure mafic granulite, similar to metamorphic zircons in the Hengshan high-pressure mafic granulites (table 11; Kröner and others, 2005a, 2005b, 2006). Finally, igneous zircons from the anatectic Huai'an charnockite and Dapinggou garnet-bearing Kf-granite yielded ages of 1849 ± 10 Ma and 1850 ± 17 Ma, respectively. All these data demonstrate that the Huai'an Complex, like other metamorphic complexes in the TNCO, underwent regional metamorphism at ~1850 Ma. Therefore, the major tectono-thermal event related to collision of the Eastern and Western Blocks to finally consolidate the basement of the North China Craton occurred at ~1.85 Ga.

ACKNOWLEDGMENTS

This paper honors the distinguished geologist Dunyi Liu, on the occasion of his 70th birthday (2007), with contributions to geochronology in China. This research was funded by the Chinese National 973 Program (2007CB411307), Chinese NSFC Grant (40730315), 111 Program (B07011) from the China Ministry of Education, and Hong Kong RGC grants (HKU7058/04P, 7055/05P, 7063/06P and 7066/07P). The study was also partly supported by the CAS/SAFEA International Partnership Program for Creative Research Teams. We thank journal reviewer M. Santosh for his constructive comments on this paper. This is The Institute for Geoscience Research (TIGeR) Publication No. 71.

References

Bai, J., 1986, The Precambrian crustal evolution of the Wutaishan area, *in* Bai, J., editor, The Early Precambrian Geology of Wutaishan: Tianjin, Tianjin Science and Technology Press, p. 376–383 (in Chinese).

Bai, J., and Dai, F. Y., 1998, Archean crust of China, *in* Ma, X. Y., and Bai, J., editors, Precambrian crust evolution of China: Beijing, Springer–Geological Publishing House, p. 15–86.

Bai, J., Wang, R. Z., and Guo, J. J., 1992, The Major Geologic Events of Early Precambrian and Their Dating in Wutaishan Region: Beijing, Geological Publishing House, 63 p.

Bingen, B., Mansfeld, J., Singmond, E. M. D., and Stein, H., 2002, Baltica-Laurentia link during the Mesoproterozoic: 1.27 Ga development of continental basins in the Sveconorwegian Orogen, southern Norway: Canadian Journal of Earth Sciences, v. 39, p. 1425–1440.

Dalziel, I. W. D., 1997, Neoproterozoic-Paleozoic geography and tectonics: review, hypothesis, environmental speculation: Geological Society of America Bulletin, v. 108, p. 16–42.

De Laeter, J. R., and Kennedy, A. K., 1998, A double focusing mass spectrometer for geochronology: International Journal of Mass Spectrum, v. 178, p. 43–50.

Dirks, P. H. G. M., Zhang, J. S., and Passchier, C. W., 1997, Exhumation of high-pressure granulites and the role of lower crustal advection in the North China Craton near Datong: Journal of Structural Geology, v. 19, p. 1343–1358.

Geng, Y. S., Wan, Y. S., Shen, Q. H., and Zhang, R. X., 2000, Early Precambrian geological events and geochronological framework of the Lüliang area: Acta Geologica Sinica, v. 74, p. 216–223.

Geraldes, M. C., Van Schmus, W. R., Condie, K. C., Bell, S., Teixeira, W., and Babinski, M., 2001, Proterozoic geologic evolution of the SW part of the Amazonian Craton in Mato Grosso state, Brazil: Precambrian Research, v. 111, p. 91–128.

Giles, D., Betts, P., and Lister, G., 2002, Far-field continental backarc setting for the 1.80-1.67 Ga basins of northeastern Australia: Geology, v. 30, p. 823–826.

Guan, H., Sun, M., Wilde, S. A., Zhou, X. H., and Zhai, M. G., 2002, SHRIMP U-Pb zircon geochronology of the Fuping Complex: implications for formation and assembly of the North China Craton: Precambrian Research, v. 113, p. 1–18.

Guo, J. H., and Shi, X., 1996, Geochronology and important geological events, *in* Zhai, M. G., editor, Granulites and lower continental crust in the North China Craton: Beijing, Seismological Press, p. 133–150 (in Chinese).

Guo, J. H., and Zhai, M. G., 2001, Sm-Nd age dating of high-pressure granulites and amphibolite from Sanggan area, North China craton: Chinese Science Bulletin, v. 46, p. 106–111.

Guo, J. H., Zhai, M. G., and Zhang, Y. G., 1993, Early Precambrian Manjinggou high-pressure granulites melange belt on the southern edge of the Huai'an Complex, North China Craton: geological features, petrology and isotopic geochronology: Acta Petrologica Sinica, v. 9, p. 329–341.

Guo, J. H., Bian, A. G., and Shi, X., 1996, High-pressure granulite, retrograde eclogite and granite in the Early Precambrian Sanggan Belt, *in* Zhai, M. G., editor, Granulites and lower continental crust in the North China Craton: Beijing, Seismological Press, p. 21–54 (in Chinese).

Guo, J. H., Zhai, M. G., and Xu, R. H., 2001, Timing of the granulite facies metamorphism in the Sanggan area, North China craton: zircon U-Pb geochronology: Science in China Series D-Earth Sciences, v. 44, p. 1010–1018.

Guo, J. H., O'Brien, P. J., and Zhai, M. G., 2002, High-pressure granulites in the Sanggan area, North China craton: metamorphic evolution, P-T paths and geotectonic significance: Journal of Metamorphic Geology, v. 20, p. 741–756.

Guo, J. H., Sun, M., Chen, F. K., and Zhai, M. G., 2005, Sm-Nd and SHRIMP U-Pb zircon geochronology of high-pressure granulites in the Sanggan area, North China Craton: Timing of Paleoproterozoic continental collision: Journal of Asian Earth Sciences, v. 24, p. 629–642.

Halls, H. C., Li, J. H., Davis, D., Hou, G., Zhang, B. X., and Qian, X. L., 2000, A precisely dated Proterozoic palaeomagnetic pole from the North China craton, and its relevance to palaeocontinental reconstruction: Geophysical Journal International, v. 143, p. 185–203.

Karlstrom, K. E., Harlan, S. S., Ahall, K. I., Williams, M. L., Mclelland, J., and Geissman, J. W., 2001, Long-lived (1.8-1.0 Ga) convergent orogen in southern Laurentia, its extensions to Australia and Baltica, and implications for refining Rodinia: Precambrian Research, v. 111, p. 5–30

Kroner, A., Compston, W., Zhang, G. W., Guo, A. L., and Cui, W. Y., 1987, Single grain zircon ages for Archean rocks from Henan, Hebei and Inner Mongolia, China, and tectonic implications: Proceeding of the International Symposium on the Tectonic Evolution and Dynamics of Continental Lithosphere, Conference Abstract Volume, Beijing, p. 24.

Kröner, A., Wilde, S. A., Li, J. H., and Wang, K. Y., 2005a, Age and evolution of a late Archaean to early Palaeozoic upper to lower crustal section in the Wutaishan/Hengshan/Fuping terrain of northern China: Journal of Asian Earth Sciences, v. 24, p. 577–595.

Kröner, A., Wilde, S. A., O'Brien, P. J., Li, J. H., Passchier, C. W., Walte, N. P., and Liu, D. Y., 2005b, Field relationships, geochemistry, zircon ages and evolution of a late Archean to Paleoproterozoic lower crustal section in the Hengshan Terrain of Northern China: Acta Geologica Sinica (English edition), v. 79, p. 605–629.

Kröner, A., Wilde, S. A., Zhao, G. C., O'Brien, P. J., Sun, M., Liu, D. Y., Wan, Y. S., Liu, S. W., and Guo, J. H., 2006, Zircon geochronology of mafic dykes in the Hengshan Complex of northern China: evidence for late Palaeoproterozoic rifting and subsequent high-pressure event in the North China Craton: Precambrian Research, v. 146, p. 45–67.

Kusky, T. M., and Li, J. H., 2003, Paleoproterozoic tectonic evolution of the North China Craton: Journal of Asian Earth Sciences, v. 22, p. 383–397.

Kusky, T. M., Li, J. H., and Santosh, M., 2007, The Paleoproterozoic North Hebei Orogen: North China craton's collisional suture with the Columbia supercontinent: Gondwana Research, v. 12, p. 4–28.

Li, J. H., and Kusky, T. M., 2007, A Late Archean foreland fold and thrust belt in the North China Craton: Implications for early collisional tectonics: Gondwana Research, v. 12, p. 47–66.

Li, J. H., and Qian, Q. L., 1991, A study on the Longquanguan shear zone in the northern part of the Taihang Mountains: Shanxi Geology, v. 6, v. 17–29 (in Chinese).

Li, J. H., Kroner, A., Qian, X. L., and Brien, P. O., 2000, Tectonic evolution of an early Precambrian high-pressure granulite belt in the North China craton: Acta Geologica Sinica-English Edition, v. 74, p. 246–258.

Li, J. L., Wang, K. Y., Wang, C. Q., Liu, X. H., and Zhao, Z. Y., 1990, An Early Proterozoic collision belt in the Wutaishan area, China: Scientia Geologica Sinica, v. 25, p. 1–11 (in Chinese).

Li, S. Z., Hao, D. F., Zhao, G. C., Sun, M., Han, Z. Z., and Guo, X. Y., 2004a, Geochemical features and origin of Dandong granite: Acta Petrologica Sinica, v. 20, p. 1417–1423.

Li, S. Z., Zhao, G. C., Sun, M., Wu, F. Y., Liu, J. Z., Hao, D. F., Han, Z. Z., and Luo, Y., 2004b, Mesozoic, not Paleoproterozoic SHRIMP U-Pb zircon ages of two Liaoji granites, Eastern Block, North China Craton: International Geology Review, v. 46, p. 162–176 (in Chinese with English abstract).

Li, S. Z., Zhao, G. C., Sun, M., Wu, F. Y., Hao, D. F., Han, Z. Z., Luo, Y., and Xia, X. P., 2005, Deformational history of the Paleoproterozoic Liaohe Group in the Eastern Block of the North China Craton: Journal of Asian Earth Science, v. 24, p. 654–669.

Li, S. Z., Zhao, G. C., Sun, M., Han, Z. Z., Zhao, G. T., and Hao, D. F., 2006, Are the South and North Liaohe Groups of the North China Craton different exotic terranes? Nd isotope constraints: Gondwana Research, v. 9, p. 198–208.

Liu, D. Y., and Geng, Y. S., 1997, Late Archean crustal accretion and reworking in northwestern Hebei Province: geochronological evidence: Acta Geoscientia Sinica, v. 18, p. 226–232 (in Chinese with English abstract).

Liu, D. Y., Page, R. W., Compston, W., and Wu, J. S., 1985, U-Pb zircon geochronology of Late Archean metamorphic rocks in the Taihangshan-Wutaishan area, North China: Precambrian Research, v. 27, p. 85–109.

Liu, F. L., ms, 1995, Metamorphic mineral-fluid evolution and tectonic environments of the granulite facies terrane in the Huaian-Datong area: Changchun, Changchun University of Earth Sciences, Ph. D. thesis, 136 p.

Liu, S. W., 1996, P-T path of the granulites in the Fuping Complex: Geological Journal of Chinese Universities, v. 2, p. 75-84 (in Chinese with English Abstract).

Liu, S. W., Shen, Q. H., and Geng, Y. S., 1996, Metamorphic evolution of two types of garnetiferous granulites from the northwestern Hebei Province and P-T estimation by the Gibbis method: Acta Petrologica Sinica, v. 12, p. 261–275.

Liu, S. W., Pan, Y. M., Li, J. H., Li, Q. G., and Zhang, J., 2002, Geological and isotopic geochemical constraints on the evolution of the Fuping Complex, North China Craton: Precambrian Research, v. 117, p. 41–56.

Liu, S. W., Pan, Y. M., Xie, Q. L., Zhang, J., and Li, Q. G., 2004, Archean geodynamics in the Central Zone, North China Craton: Constraints from geochemistry of two contrasting series of granitoids in the Fuping and Wutai Complexes: Precambrian Research, v. 130, p. 229–249.

Liu, S. W., Pan, Y. M., Xie, Q. L., Zhang, J., and Li, Q. G., 2005, Geochemistry of the Paleoproterozoic Nanying Granitoid Gneisses: constraints on the tectonic setting of the Central Zone, North China Craton: Journal of Asian Earth Sciences, v. 24, p. 643–658.

Liu, S. W., Zhao, G. C., Wilde, S. A., Shu, G. M., Sun, M., Li, Q. G., Tian, W., and Zhang, J., 2006, Th-U-Pb monazite geochronology of the Lüliang and Wutai Complexes: constraints on the tectonothermal evolution of the Trans-North China Orogen: Precambrian Research, v. 148, p. 205–225.

Liu, Y. G., ms, 1989, Origin and crustal evolution of the Northwestern Hebei metamorphic complexes: An integrated petrological, geochemical and geochronological study: Beijing, Peking University, Ph. D. thesis, 150 p.

Lu, L. Z., 1991, Metamorphic P–T–t path of the Archean granulite-facies terrains in Jining area, Inner Mongolia and its tectonic implications: Acta Petrologica Sinica, v. 8, p. 1–12.

Lu, L. Z., and Jin, S. Q., 1993, P–T–t paths and tectonic history of an early Precambrian granulite facies terrane, Jining district, southeastern Inner Mongolia, China: Journal of Metamorphic Geology, v. 11, p. 483–498.

Ludwig, K. R., 2001, Users Manual for Isoplot 3.00: a geochronological toolkit for Microsoft Excel: Berkeley, Berkeley Geochronology Center, Special Publication No. 1a, 56 p.

Ma, X. Y., Bai, J., Shuo, S. T., Lao, Q. Y., and Zhang, J. S., 1987, The Early Precambrian tectonic framework of China and research methods: Beijing, Geological Publishing Press, 131 p (in Chinese).

Mao, D. B., Zhong, C. T., Chen, Z. H., Lin, Y. X., Li, H. M., and Hu, X. D., 1999, Isotopic ages and geological implications of high-pressure mafic granulites in the northern Chengde area, Hebei Province, China: Acta Petrologica Sinica, v. 15, p. 524–534.

Mei, H. L., 1994, P-T-t path and tectonic evolution of the Palaeoproterozoic metamorphic rocks in the Zhongtiaoshan Complex: Geological Review, v. 40, p. 36–45 (in Chinese with English abstract).

Nelson, D. R., 1997, Compilation of SHRIMP U-Pb zircon geochronology data, 1996: Geological Survey of Western Australia, Record 1997/2, 189 p.

O′Brien, P. J., Walte, N., and Li, J. H., 2005, The petrology of two distinct granulite types in the Hengshan Mts, China, and tectonic implications: Journal of Asian Earth Sciences, v. 24, p. 615–627.

Pidgeon, R. T., Furfaro, D., Kennedy, A. K., Nemchin, A., van Bronswijk, W., and Todt, W. A., 1994, Calibration of zircon standards for the Curtin SHRIMP II: Berkeley, Eighth International Conference on Geochronology, Cosmochronology and Isotope Geology, Abstract, U.S. Geological Survey Circular, 1107, p. 251.

Polat, A., Kusky, T. M., Li, J. H., Fryer, B., Kerrich, R., and Patrick, K., 2005, Geochemistry of Neoarchean (ca. 2.55–2.50 Ga) volcanic and ophiolitic rocks in the Wutaishan greenstone belt, central orogenic belt, North China Craton: Implications for geodynamic setting and continental growth: Geological Society of America Bulletin, v. 117, p. 1387–1399.

Rivers, T., and Corrigan, D., 2000, Convergent margin on southeastern Laurentia during the Mesoproterozoic: tectonic implications: Canadian Journal of Earth Sciences, v. 37, p. 359–383.

Santosh, M., Sajeev, K., and Li, J. H., 2006, Extreme crustal metamorphism during Columbia supercontinent assembly: Evidence from North China Craton: Gondwana Research, v. 10, p. 256–266.

Santosh, M., Tsunogae, T., and Li, J. H., 2007, Discovery of sapphirine-bearing Mg–Al granulites in the North China Craton: Implications for Paleoproterozoic ultrahigh temperature metamorphism: Gondwana Research, v. 11, p. 263–285.

Steiger, R. H., and Jäger, E., 1977, Subcommission on geochronology: convention on the use of decay constants in geo- and cosmochronology: Earth and Planetary Science Letters, v. 36, p. 359–362.

Tian, W., Liu, S. W., Liu, C. H., Yu, S. Q., Li, Q. G., and Wang, Y. R., 2005, SHRIMP U-Pb zircon ages and geochemistry of the Sushui TTG gneisses in the Zhongtiao Complex and their geological significance: Progress in Natural Science, v. 15, p. 1476–1484.

Tian, Y. Q., 1991, Geology and Mineralization of Wutai–Hengshan Greenstone Belt: Taiyuan, Shanxi Science and Technology Press, 244 p (in Chinese).

Wan, Y. S., Wilde, S. A., Liu, D. Y., Yang, C. X., Song, B., and Yin, X. Y., 2006, Further evidence for ~1.85 Ga metamorphism in the Central Zone of the North China Craton: SHRIMP U-Pb dating of zircon from metamorphic rocks in the Lushan area, Henan Province: Gondwana Research, v. 9, p. 189–197.

Wang, K. Y., Li, J. L., Hao, J., Li, J. H., and Zhou, S. P., 1996, The Wutaishan mountain belt within the Shanxi Province, Northern China: a record of late Archean collision tectonics: Precambrian Research, v. 78, p. 95–103.

——— 1997, Late Archean mafic-ultramafic rocks from the Wuatishan, Shanxi Province: a possible ophiolite mélange: Acta Petrologica Sinica, v. 13, p. 139–151.

Wang, K. Y., Wang, Z. H., Yu, L. J., Fan, H. R., Wilde, S. A., and Cawood, P. A., 2001, Evolution of Archaean greenstone belt in the Wutaishan region, North China: constraints from SHRIMP zircon U-Pb and other geochronological and isotope information: Perth, AGSO - Geoscience Australia, Record, v. 37, p. 104–105.

Wang, Y. J., Fan, W. M., Zhang, Y., and Guo, F., 2003, Structural evolution and $^{40}Ar/^{39}Ar$ dating of the Zanhuang metamorphic domain in the North China Craton: constraints on Paleoproterozoic tectonothermal overprinting: Precambrian Research, v. 122, p. 159–182.

Wang, Y. J., Fan, W. M., Zhang, Y., Guo, F., Zhang, H., and Peng, T. P., 2004, Geochemical $^{40}Ar/^{39}Ar$ geochronological and Sr-Nd isotopic constraints on the origin of Paleoproterozoic mafic dikes from the southern Taihang Mountains and implications for the ca. 1800 Ma event of the North China Craton: Precambrian Research, v. 135, p. 55–77.

Wang, Y. J., Zhao, G. C., Fan, W. M., Peng, T. P., Sun, L. H., and Xia, X. P., 2007, LA-ICP-MS U-Pb zircon geochronology and geochemistry of Paleoproterozoic mafic dikes from western Shandong Province: Implications for back-arc basin magmatism in the Eastern North China Craton: Precambrian Research, v. 154, p. 107–124.

Wilde, S., 2002, SHRIMP U-Pb zircon ages of the Wutai Complex, *in* Kröner, A., Zhao, G. C., Wilde, S. A., Zhai, M. G., Passchier, C. W., Sun, M., Guo, J. H., O'Brien, P. J., and Walte, N., editors, A Late Archaean to Palaeoproterozoic Lower to Upper Crustal Section in the Hengshan-Wutaishan Area of North China, Guidebook for Penrose Conference Field Trip: Beijing, Chinese Academy of Sciences, p. 32–34.

Wilde, S. A., and Zhao, G. C., 2005, Archean to Paleoproterozoic evolution of the North China Craton: Journal of Asian Earth Sciences, v. 24, p. 520–523.

Wilde, S. A., Cawood, P., Wang, K. Y., and Nemchin, A., 1997, The relationship and timing of granitoid evolution with respect to felsic volcanism in the Wutai Complex, North China craton: Proceedings of the 30th International Geological Conference: Precambrian Geology and Metamorphic Petrology, v. 17, p. 75–88.

Wilde, S. A., Zhao, G. C., and Sun, M., 2002, Development of the North China Craton during the late Archaean and its final amalgamation at 1.8 Ga: Some speculations on its position within a global Palaeoproterozoic supercontinent: Gondwana Research, v. 5, p. 85–94.

Wilde, S. A., Zhao, G. C., Wang, K. Y., and Sun, M., 2004a, First precise SHRIMP U-Pb zircon ages for the Hutuo Group, Wutaishan: further evidence for the Palaeoproterozoic amalgamation of the North China Craton: Chinese Science Bulletin, v. 49, p. 83–90.

Wilde, S. A., Cawood, P. A., Wang, K. Y., Nemchin, A., and Zhao, G. C., 2004b, Determining Precambrian crustal evolution in China: a case-study from Wutaishan, Shanxi Province, demonstrating the application of precise SHRIMP U-Pb geochronology, *in* Malps, J., Fletcher, C. J., Ali, J. R., and Aitchison, J. C., editor, Aspects of the Tectonic Evolution of China: London, Geological Society Special Publication, No. 226, p. 5–26.

Wilde, S. A., Cawood, P. A., Wang, K. Y., and Nemchin, A. A., 2005. Granitoid evolution in the late Archean Wutai Complex, North China Craton: Journal of Asian Earth Sciences, v. 24, p. 520–520.

Wu, C. H., and Zhong, C. T., 1998, The Paleoproterozoic SW–NE collision model for the central North China Craton: Progress of Precambrian Research, v. 21, p. 28–50 (in Chinese).

Wu, F. Y., Zhao, G. C., Wilde, S. A., and Sun, D. Y., 2005, Nd isotopic constraints on crustal formation in the North China Craton: Journal of Asian Earth Sciences, v. 24, p. 524–546.

Wu, J. S., Geng, Y. S., Xu, H. F., Jin, L. G., He, S. Y., and Sun, S. W., 1989, Metamorphic geology of Fuping Group: Journal of Chinese Institute of Geology, v. 19, p. 1–213 (in Chinese).

Zhai, M. G., Guo, J. H., Yan, Y. H., Li, Y. G., and Han, X. L., 1993, Discovery of high-pressure basic granulite terrain in the North China Craton: A preliminary study: Science in China Series B-Chemistry, v. 36, p. 1402–1408.

Zhai, M. G., Guo, J. H., Li, J. H., Li, Y. G., Yan, Y. H., and Zhang, W. H., 1996, Retrograded eclogites in the Archaean North China Craton and their geological implication: Chinese Science Bulletin, v. 41, p. 315–320.

Zhang, J., Zhao, G. C., Sun, M., Wilde, S. A., Li, S. Z., and Liu, S. W., 2006, High-pressure mafic granulites in the Trans-North China Orogen: Tectonic significance and age: Gondwana Research, v. 9, p. 349–362.

Zhang, J., Zhao, G. C., Li, S. Z., Sun, M., Liu, S. W., Wilde, S. A., Kroner, A., and Yin, C. Q., 2007, Deformation history of the Hengshan Complex: implications for the tectonic evolution of the Trans-North China Orogen: Journal of Structural Geology, v. 29, p. 933–949.

Zhang, J. S., Dirks, H. G. M., and Passchier, C. W., 1994, Extensional collapse and uplift in a polymetamorphic granulite terrain in the Archean and Paleoproterozoic of north China: Precambrian Research, v. 67, p. 37–57.

Zhao, G. C., 2001, Palaeoproterozoic assembly of the North China Craton: Geological Magazine, v. 138, p. 87–91.

Zhao, G. C., Wilde, S. A., Cawood, P. A., and Lu, L. Z., 1998, Thermal evolution of Archean basement rocks from the eastern part of the North China carton and its bearing on tectonic setting: International Geology Review, v. 40, p. 706–721.

——— 1999a, Tectonothermal history of the basement rocks in the western zone of the North China Craton and its tectonic implications: Tectonophysics, v. 310, p. 37–53.

Zhao, G. C., Cawood, P. A., and Lu, L. Z., 1999b, Petrology and P-T history of the Wutai amphibolites: implications for tectonic evolution of the Wutai Complex, China: Precambrian Research, v. 93, p.181–199.

Zhao, G. C., Wilde, S. A., Cawood, P. A., and Lu, L. Z., 1999c. Thermal evolution of two types of mafic granulites from the North China craton: implications for both mantle plume and collisional tectonics: Geological Magazine, v. 136, p. 223–240.

Zhao, G. C., Cawood, P. A., Wilde, S. A., Min, S., and Lu, L. Z., 2000a, Metamorphism of basement rocks in the Central Zone of the North China Craton: implications for Paleoproterozoic tectonic evolution: Precambrian Research, v. 103, p. 55–88.

Zhao, G. C., Wilde, S. A., Cawood, P. A., and Lu, L. Z., 2000b, Petrology and P-T path of the Fuping mafic granulites: implications for tectonic evolution of the central zone of the North China craton: Journal of Metamorphic Geology, v. 18, p. 375–391.

Zhao, G. C., Wilde, S. A., Cawood, P. A., and Sun, M., 2001a, Archean blocks and their boundaries in the North China Craton: lithological, geochemical, structural and P-T path constraints and tectonic evolution: Precambrian Research, v. 107, p. 45–73.

Zhao, G. C., Cawood, P. A., Wilde, S. A., and Lu, L. Z., 2001b, High-pressure granulites (retrograded eclogites) from the Hengshan Complex, North China Craton: Petrology and tectonic implications: Journal of Petrology, v. 42, p. 1141–1170.

Zhao, G. C., Wilde, S. A., Cawood, P. A., and Sun, M., 2002, SHRIMP U-Pb zircon ages of the Fuping Complex: Implications for late Archean to Paleoproterozoic accretion and assembly of the North China Craton: American Journal of Science, v. 302, p. 191–226.

Zhao, G. C., Sun, M., and Wilde, S. A., 2003, Major tectonic units of the North China Craton and their Paleoproterozoic assembly: Science in China Series D-Earth Sciences, v. 46, p. 23–38.

Zhao, G. C., Sun, M., Wilde, S. A., and Li, S. Z., 2005, Late Archean to Paleoproterozoic evolution of the North China Craton: key issues revisited; Precambrian Research, v. 136, p. 177–202.

Zhao, G. C., Kröner, A., Wilde, S. A., Sun, M., Li, S. Z., Li, X. P., Zhang, J., Xia, X. P., and He, Y. H., 2007, Lithotectonic elements and geological events in the Hengshan-Wutai-Fuping belt: A synthesis and implications for the evolution of the Trans-North China Orogen: Geological Magazine, v. 144, p. 753–775.

Zhao, G. C., Wilde, S. A., Sun, M., Li, S. Z., Li, X. P., and Zhang, J., 2008, SHRIMP U-Pb zircon ages of granitoid rocks in the Lüliang Complex: Implications for the accretion and evolution of the Trans-North China Orogen: Precambrian Research, v. 160, p. 213–226.